VHE Pulsed Emissions from Rotation-Powered Pulsar

HIROTANI, Kouichi

ASIAA/TIARA-NTHU, Taiwan

CTA Workshop
Kashiwa, Japan
September 25, 2012

Crab nebula: Composite image of X-ray [blue] and optical [red]

§1 γ-ray Pulsar Observations

After 2008, LAT aboard Fermi has detected more than 121 pulsars above 100 MeV.

Large Area Telescope

Fermi γ-ray space telescope

Fermi/LAT point sources (>100 MeV)

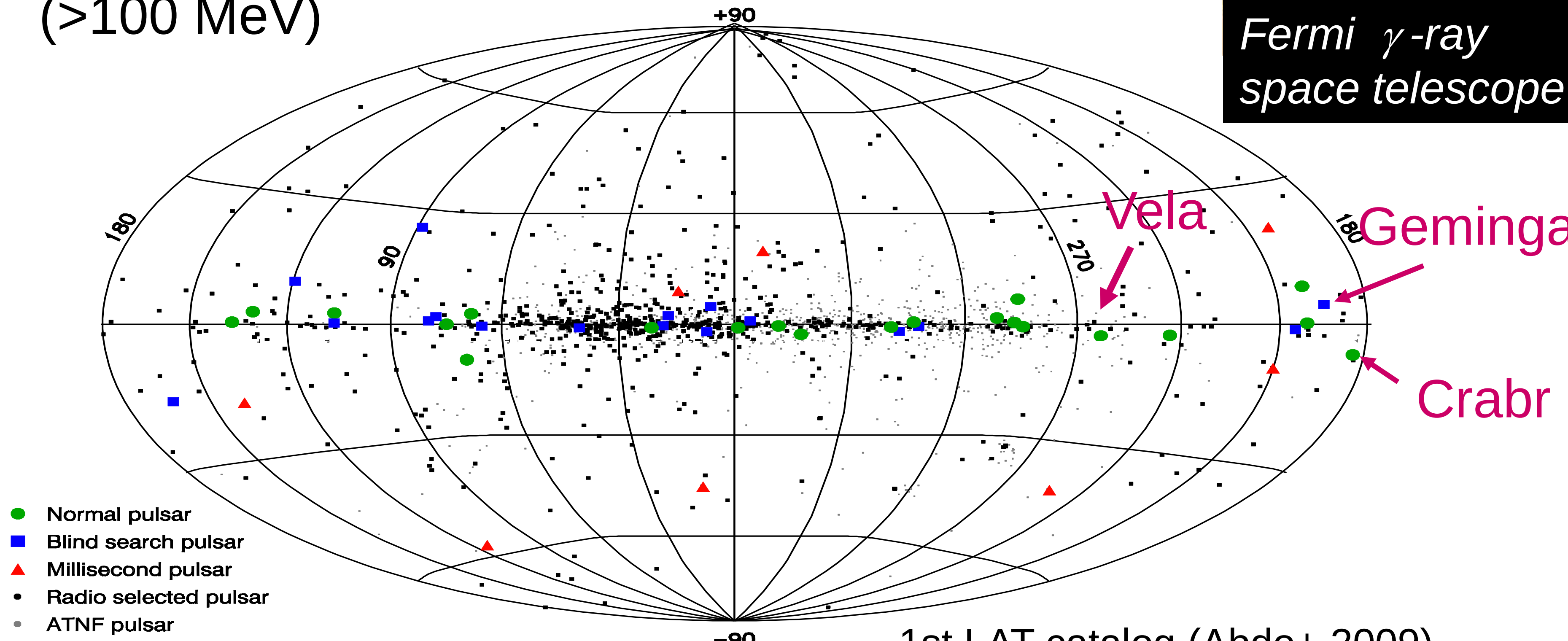

1st LAT catalog (Abdo+ 2009)

§1 γ-ray Pulsar Observations

Recent IACTs found pulsed emission in 25-400 GeV from the Crab pulsar.

VERITAS (> 120 GeV)

Aliu+ (2011, Science 334, 69)

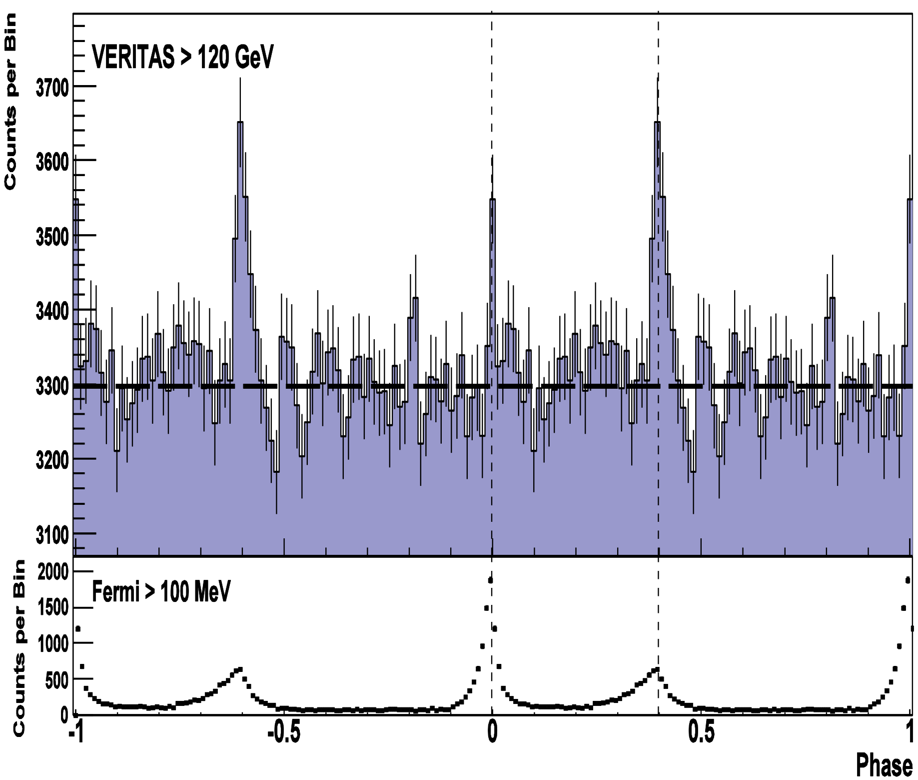

MAGIC (25−416 GeV)

Aleksić+ (2011a,b)

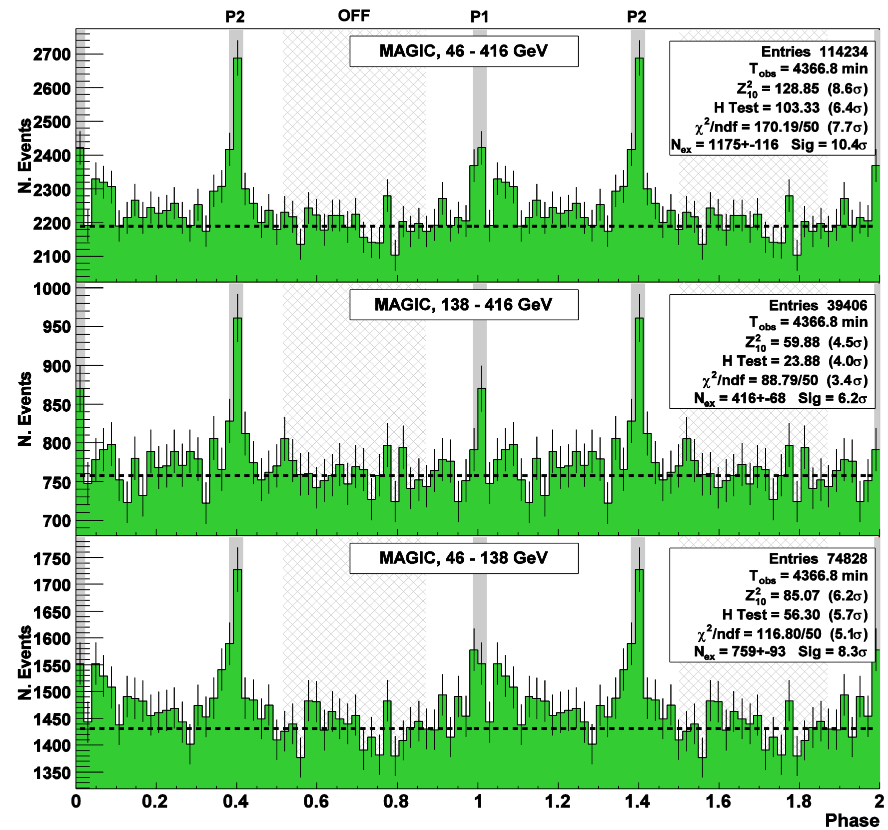

Broad-band spectra (pulsed)

- High-energy (> 100MeV) photons are emitted mainly via **curvature** process by ultra-relativistic (~10 TeV) $e^{\pm}$'s accelerated in pulsar magnetosphere.

- Above 20 GeV, **ICS by secondary/tertiary pairs** contributes.

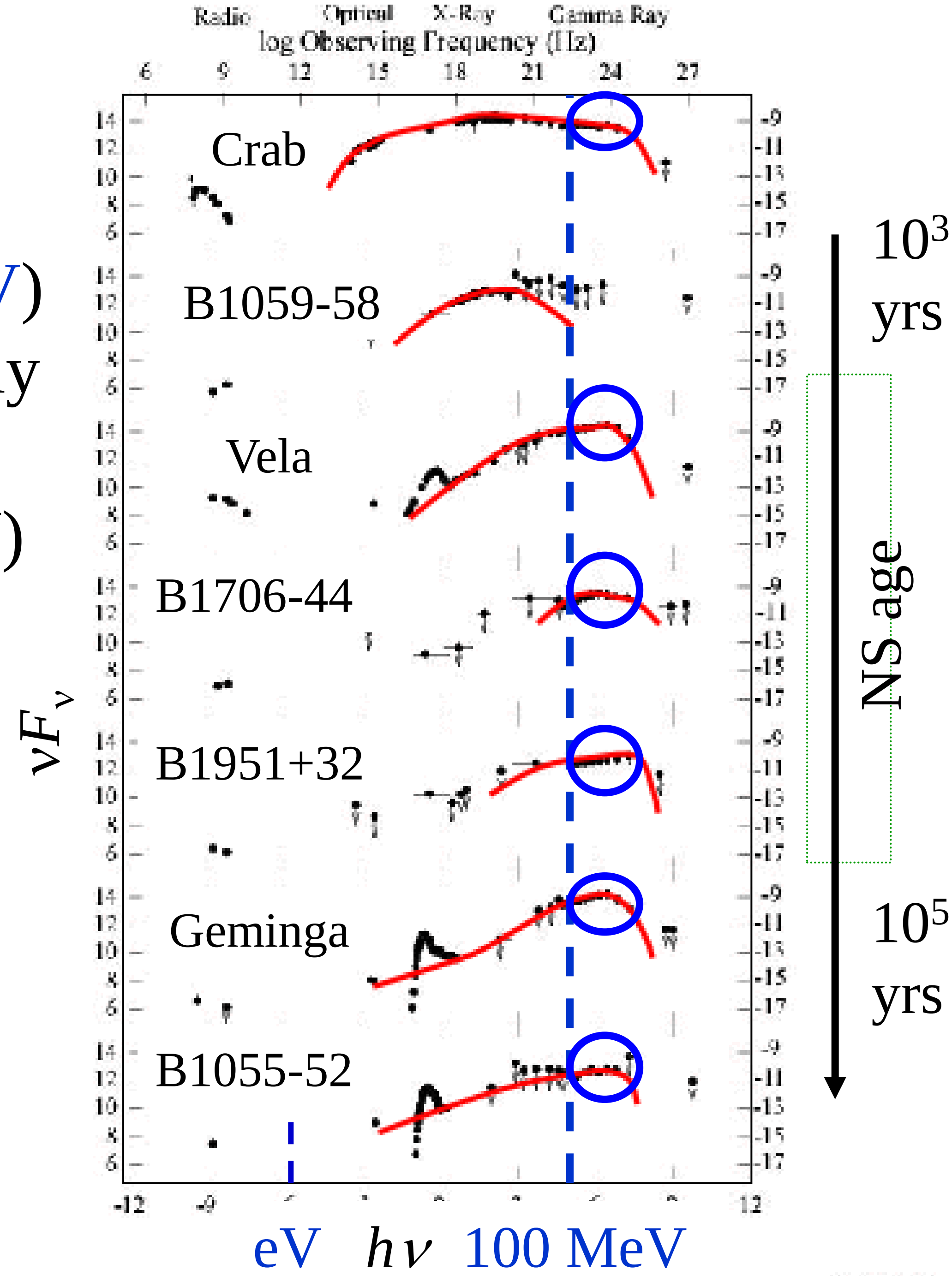

Broad-band spectra (pulsed)

- High-energy (> 100MeV) photons are emitted mainly via **curvature** process by ultra-relativistic (~10 TeV) $e^{\pm}$'s accelerated in pulsar magnetosphere.

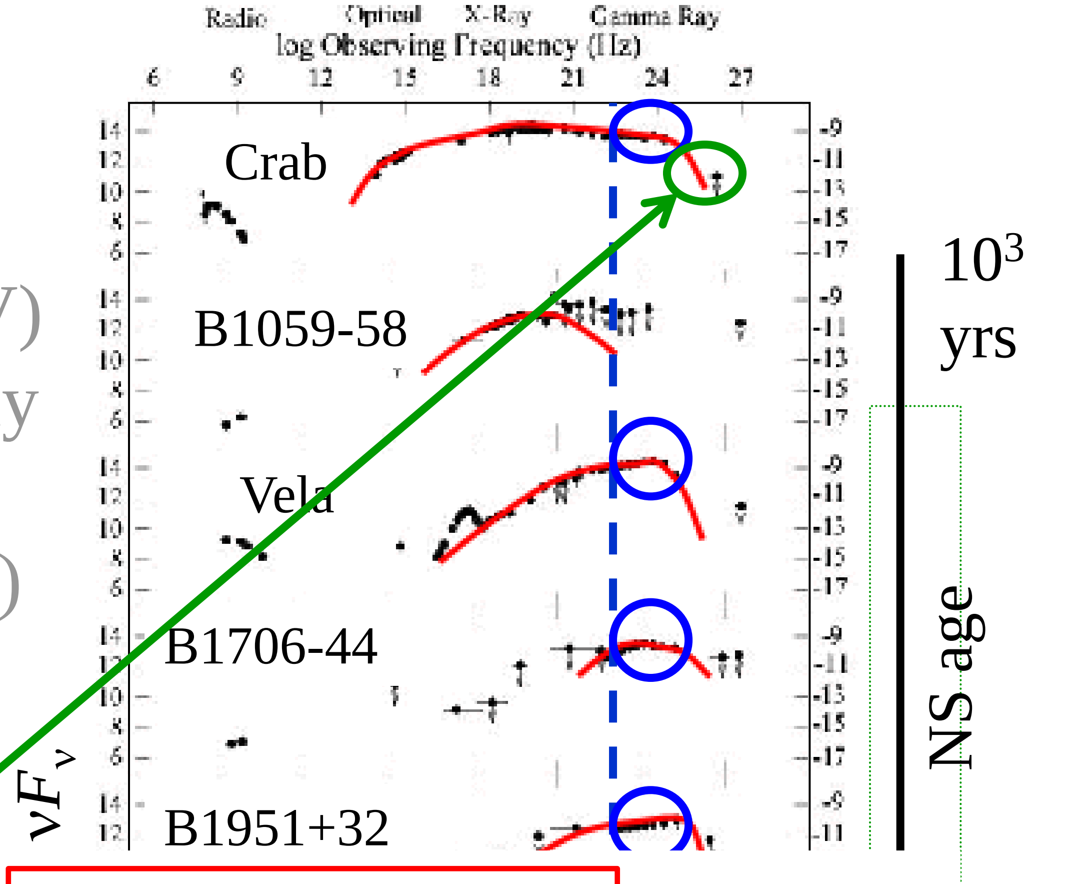

- Above 20 GeV, **ICS by secondary/tertiary pairs** contributes.

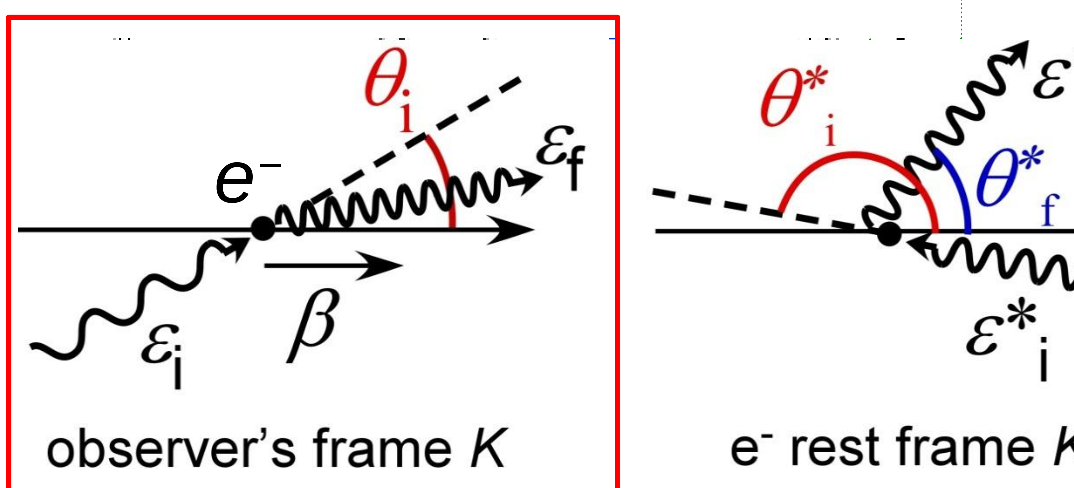

Broad-band spectra (pulsed)

- High-energy (> 100MeV) photons are emitted mainly via **curvature** process by ultra-relativistic (~10 TeV) $e^{\pm}$'s accelerated in pulsar magnetosphere.

- Some of the **primary** γ-rays are absorbed in the NS magnetosphere and reprocessed in lower energies via **synchrotron** process.

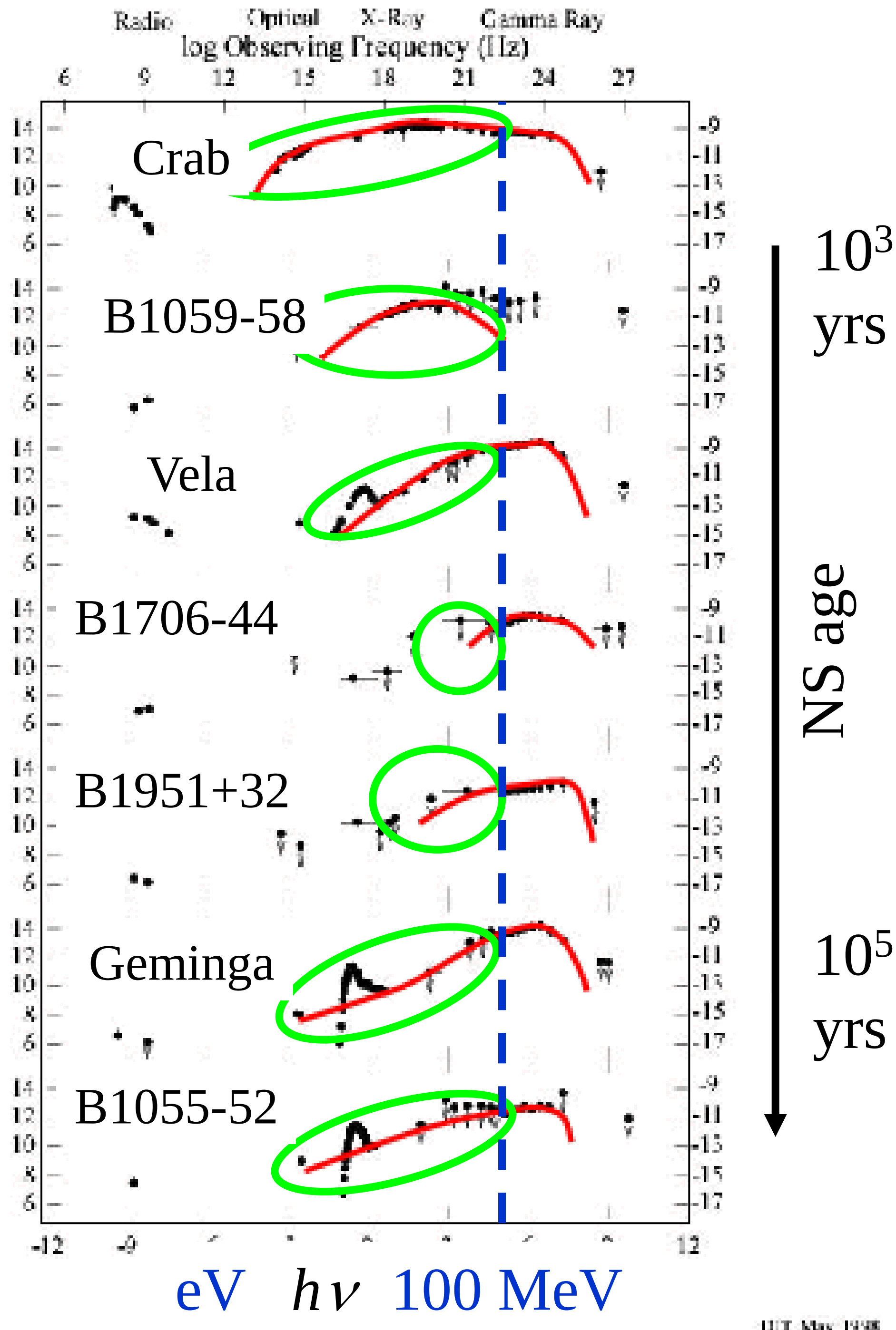

§2 Rotating NS Magnetosphere

The observed high-energy emissions are realized when the rotational energy of the NS is electro-dynamically extracted and partly dissipated in its magnetosphere.

(e.g., unipolar inductor)

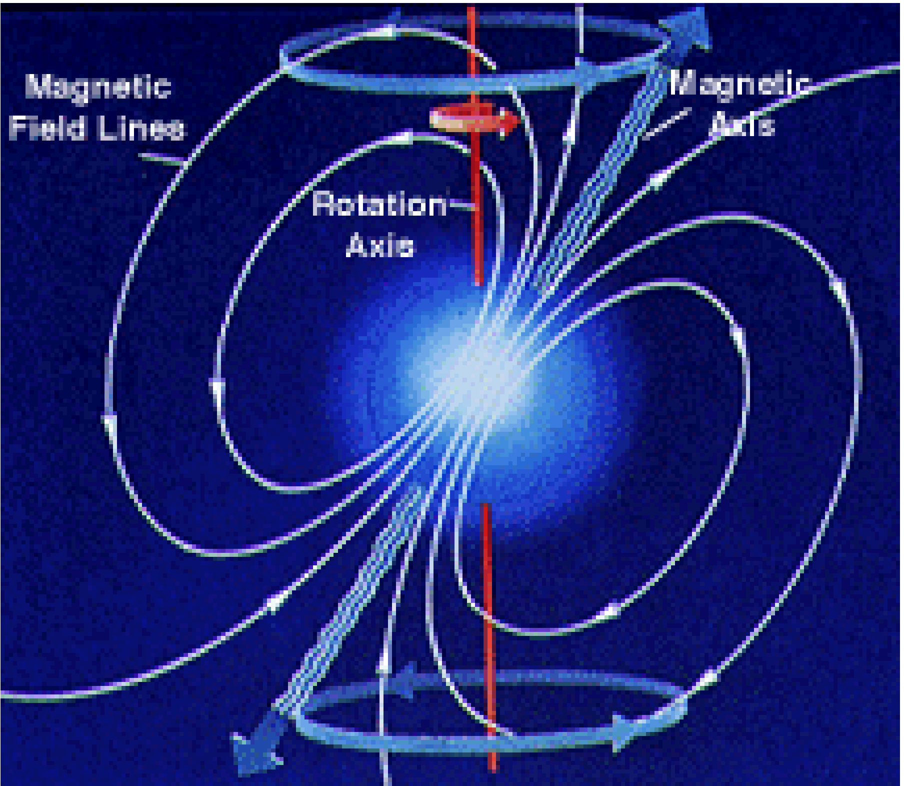

Magnetic and rotation axes are generally misaligned.

Pulsars:

rapidly rotating, highly magnetized NS

§2 Rotating NS Magnetosphere

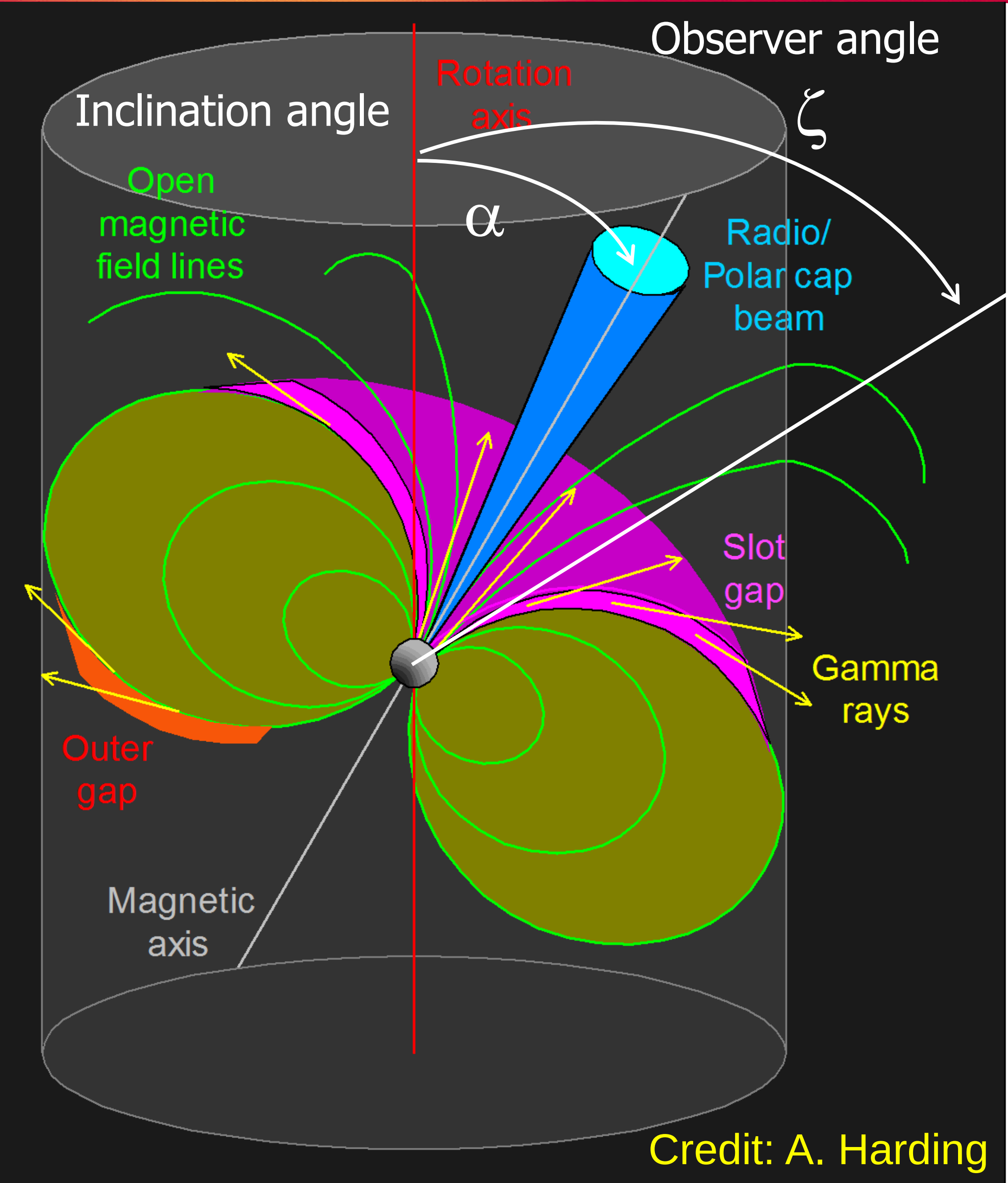

Possible sites of particle acceleration

- Ideal MHD condition holds in most of magnetosphere,
$$E \bullet B = 0.$$
- In some limited regions, deficient charge supply leads to $E \bullet B \neq 0$.
- In charge deficit region, $E_{\parallel}$ is solved from the Poisson eq.,
$$\nabla \bullet E_{\parallel} = 4\pi(\rho - \rho_{GJ}).$$

§2 Rotating NS Magnetosphere

Early 80's, the polar-cap (PC) model was proposed.

(Daugherty & Harding ApJ 252, 337, 1982)

A single PC beam can produce a variety of pulse profiles.

However, the emission solid angle ($\Delta\Omega$ «1 ster) was too small to reproduce the wide-separated double peaks.

A great deal of effort has been made; however, one has to invoke a very small inclination, α, and viewing angles, ζ, to reproduce the widely separated pulse peaks.

In addition, localization of gap altitudes («r_*) prohibits enough L_γ ($<0.3L_{\rm spin}$) as observed. ($L_{\rm radio}\sim 10^{-5}L_{\rm spin}$ is OK.)

Thus, a high-altitude emission drew attention.

§3 Higher-altitude Pulsar Emission Models

Big breakthrough: Muslimov & Tsygan (1992, MN 255, 61) found that a polar gap can extend into the higher altitudes by virtue of the frame-dragging effect.

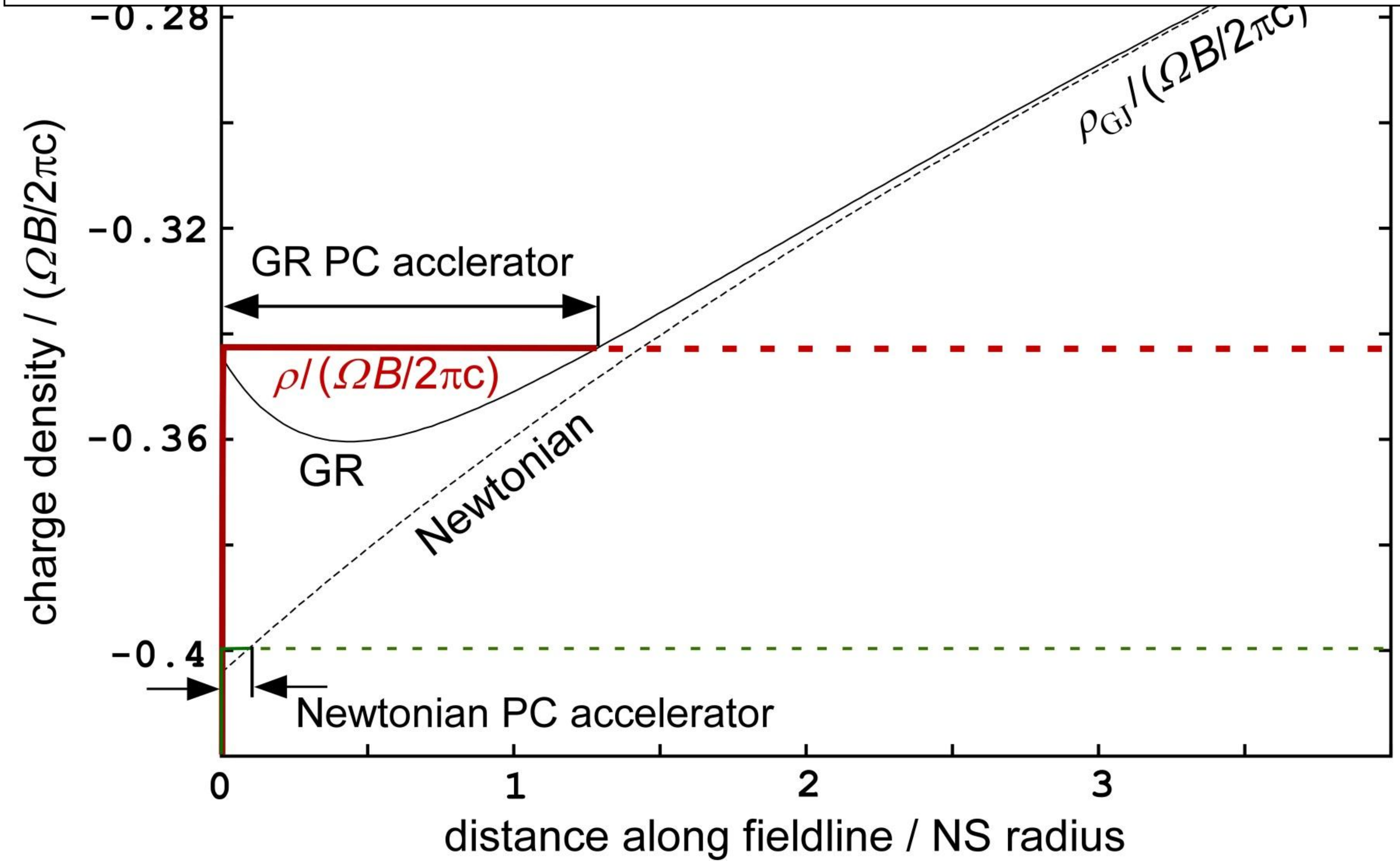

§3 Higher-altitude Pulsar Emission Models

Extending the original idea of Arons (1983, ApJ 266, 215), Muslimov & Harding (2003, ApJ 588, 430) proposed the lower-altitude slot-gap (SG) model.

Slot gap = a pair-free space formed between the last-open field lines and the pair-formation front (PFF).

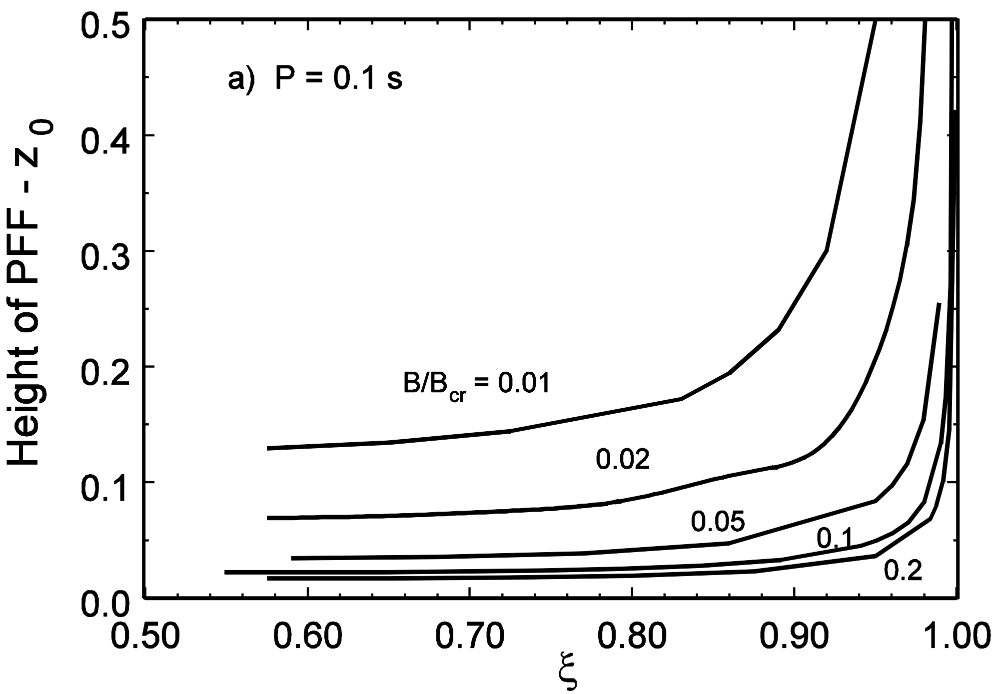

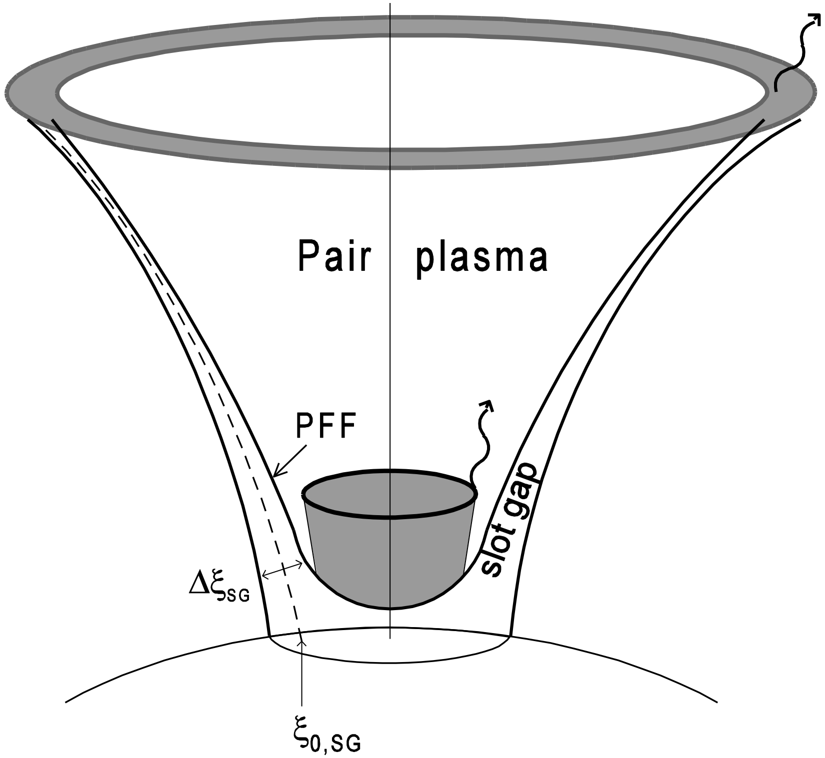

§3 Higher-altitude Pulsar Emission Models

However, a lower-altitude SG is still limited within a few r_*.

Thus, the same difficulty ($\Delta\Omega$ «1 ster) still remains.

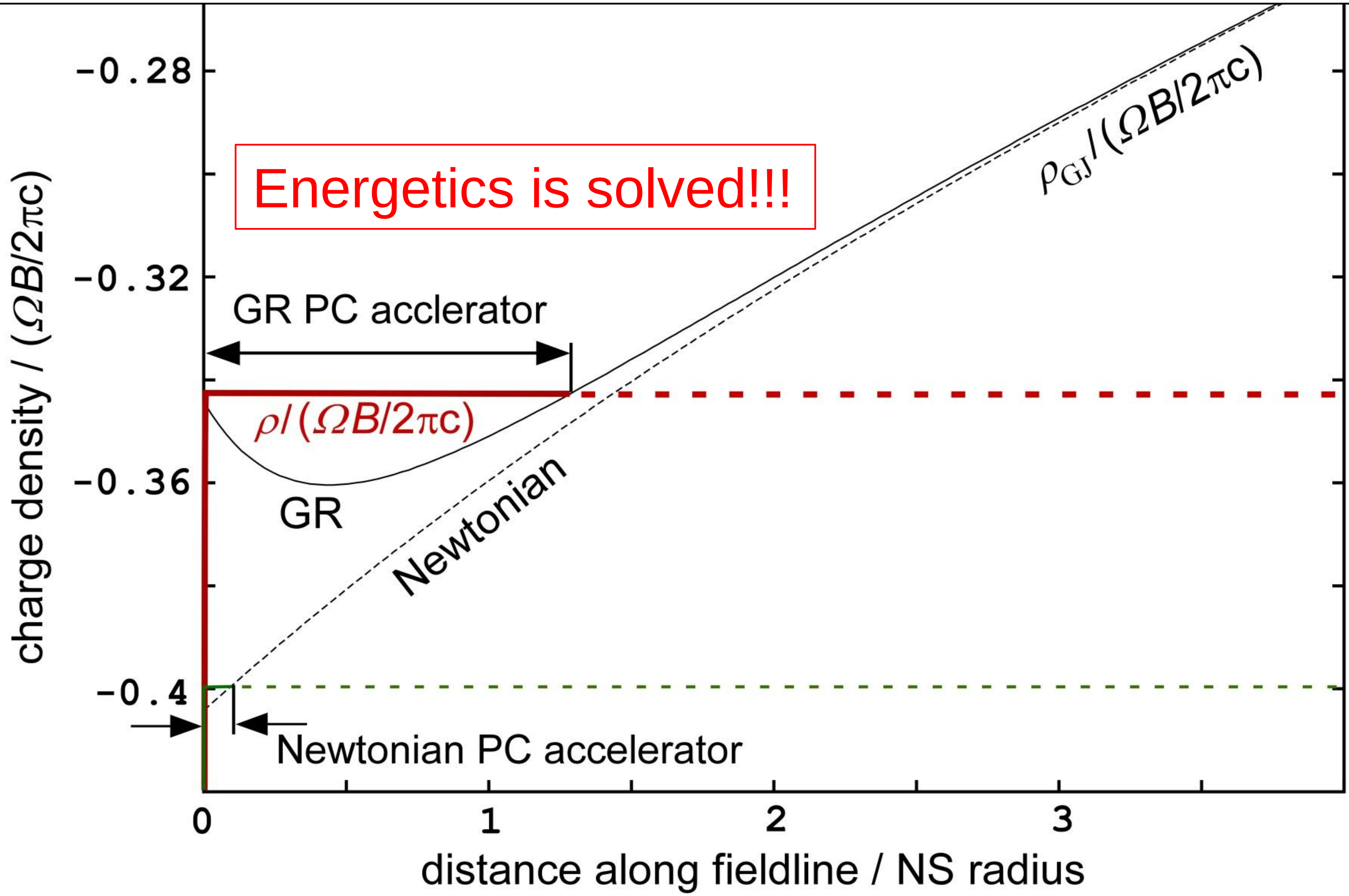

§3 Higher-altitude Pulsar Emission Models

To contrive a higher-altitude emission model, Muslimov & Harding (2004a, ApJ 606, 1143; 2004b, ApJ 617, 471) and Dyks, Harding & Rudak (2004, ApJ 606, 1125) extended the lower-altitude slot-gap solution into higher altitudes (in fact, by hand).

They explained, e.g., the widely separated double peaks.

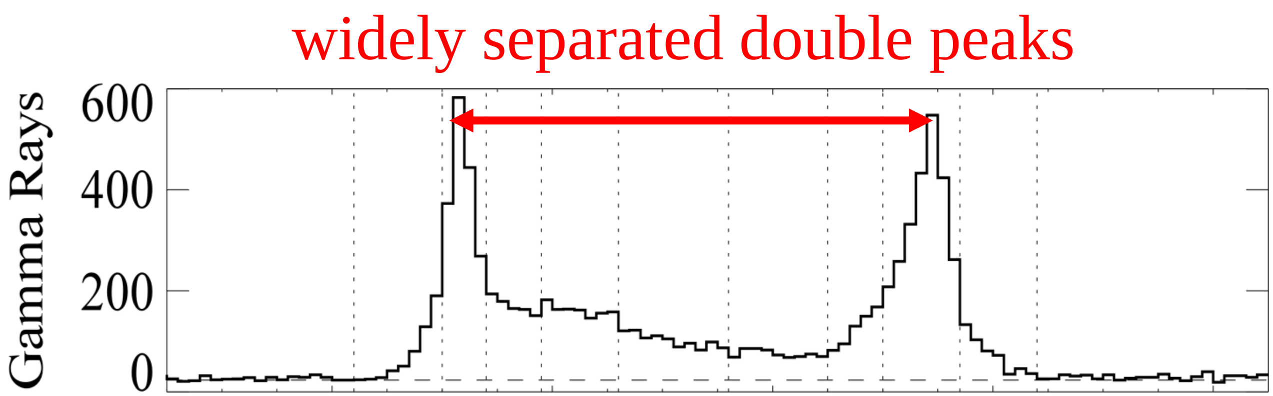

§3 Higher-altitude Pulsar Emission Models

Assuming that the gap extends from the NS surface to the light cylinder with constant emissivity, Dyks & Rudak (2003, ApJ 598, 1201) demonstrated the formation of double peaks, which arise from the crossing of two caustics associated with different poles.

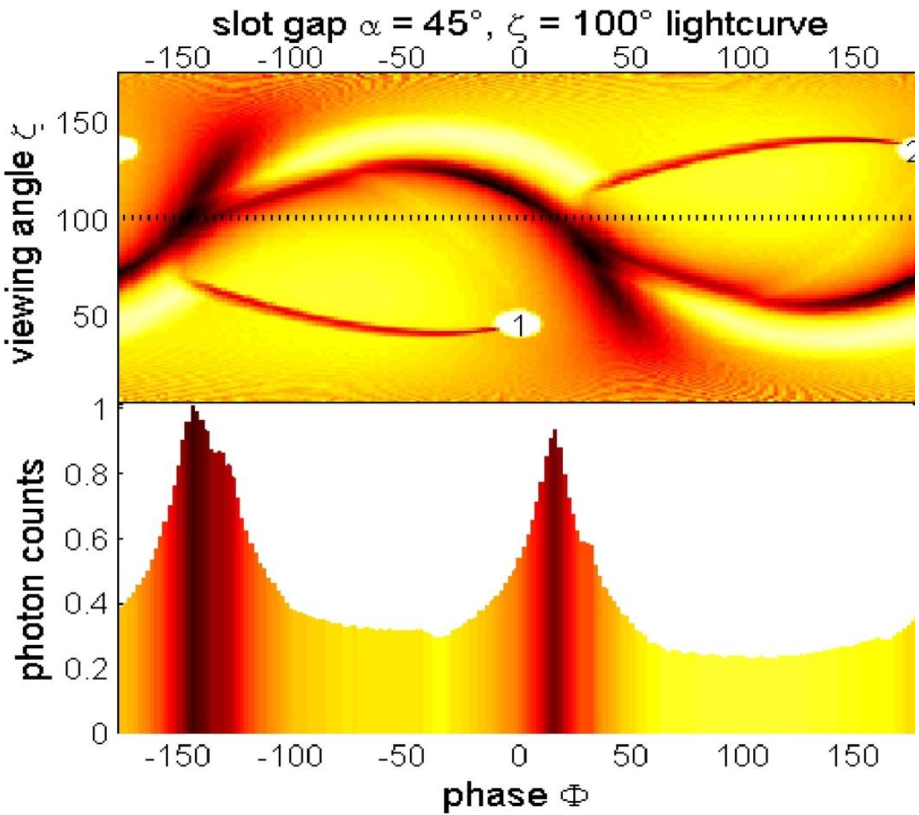

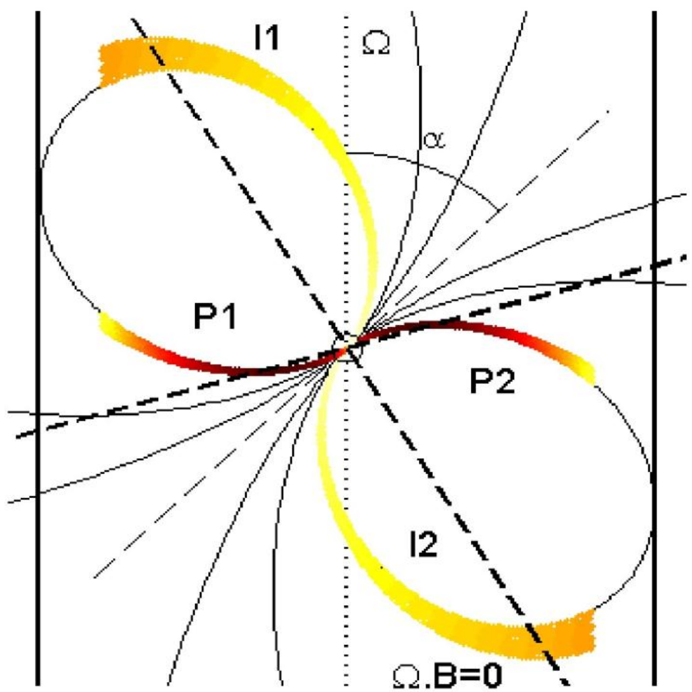

§3 Higher-altitude Pulsar Emission Models

Assuming that the gap extends from the NS surface to the light cylinder with constant emissivity, Dyks & Rudak (2003, ApJ 598, 1201) demonstrated the formation of double peaks.

In this higher-altitude slot-gap model, most observers catch emission from both (N/S) poles.

trailing-side emission $\longrightarrow$ main peaks
leading-side emission $\longrightarrow$ inter-peak & off-pulse

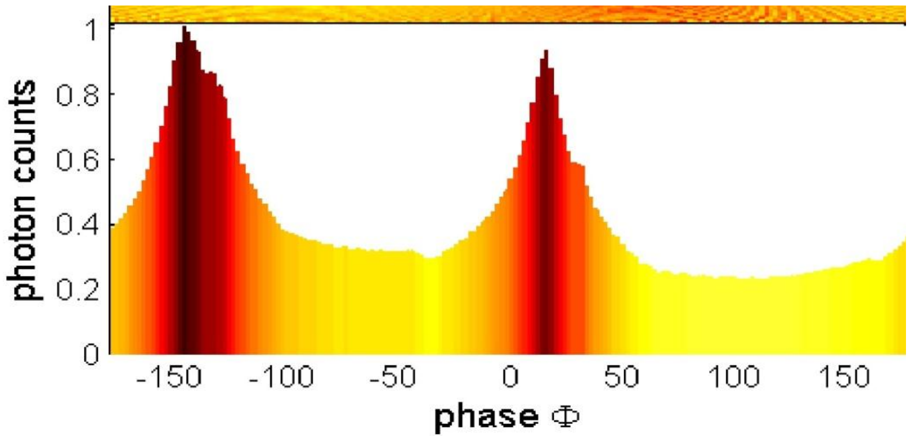

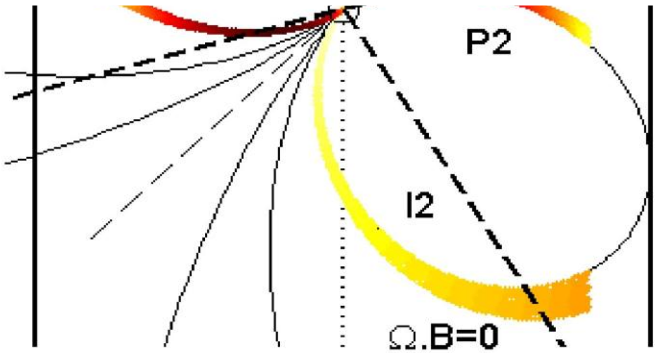

§3 Higher-altitude Pulsar Emission Models

Dyks, Harding, Rudak (2004, ApJ 606, 1125) showed that Crab pulsar's optical polarization characteristics can be qualitatively reproduced by their SG model.

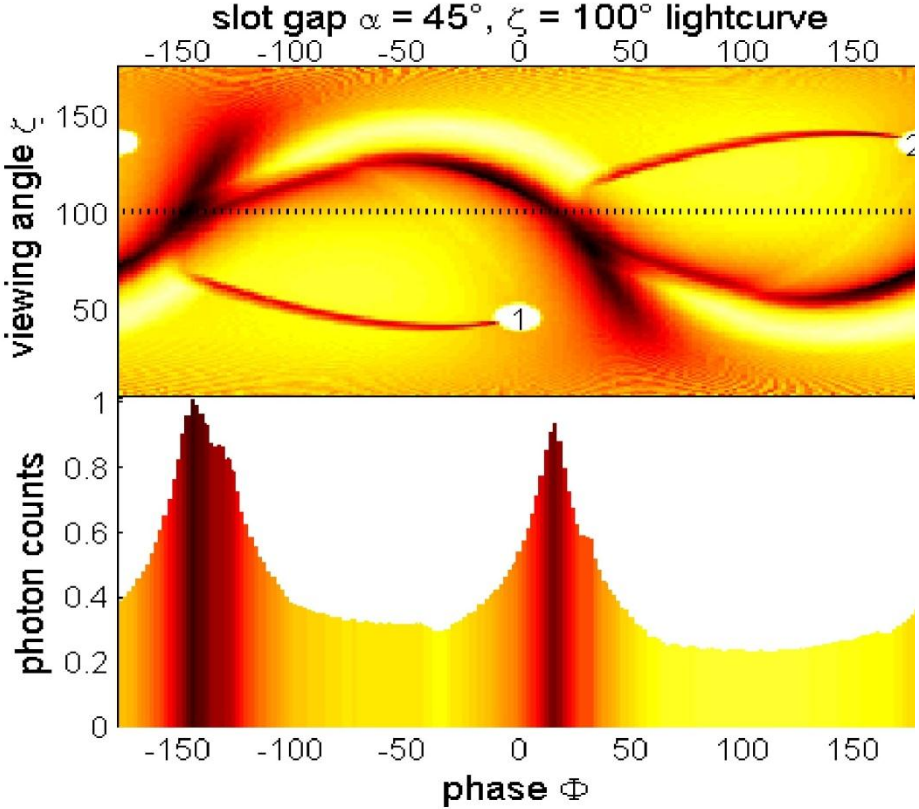

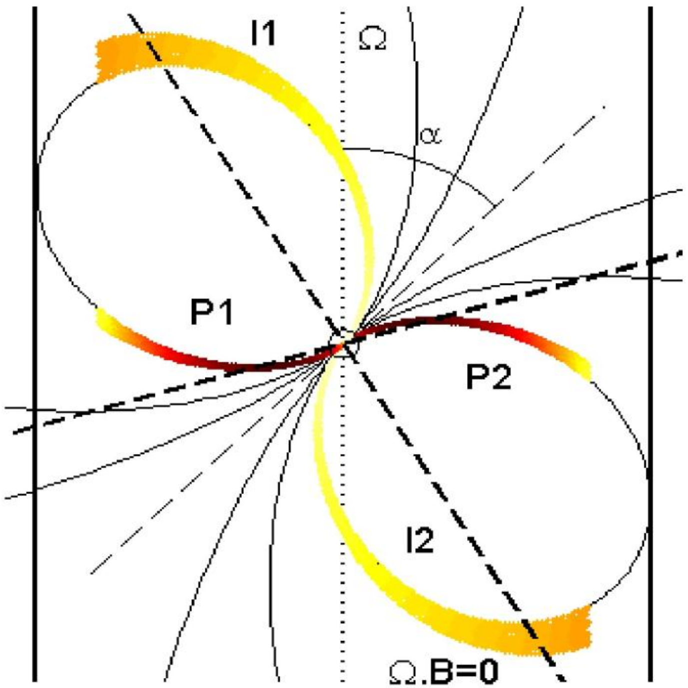

§3 Higher-altitude Pulsar Emission Models

Dyks, Harding, Rudak (2004, ApJ 606, 1125) showed that Crab pulsar's optical polarization characteristics can be qualitatively reproduced by their SG model.

Harding+ (2008, ApJ ApJ 680, 1378) examined Crab's γ-ray emission and found that the pulse profiles and the phase-resolved spectrum are qualitatively reproduced.

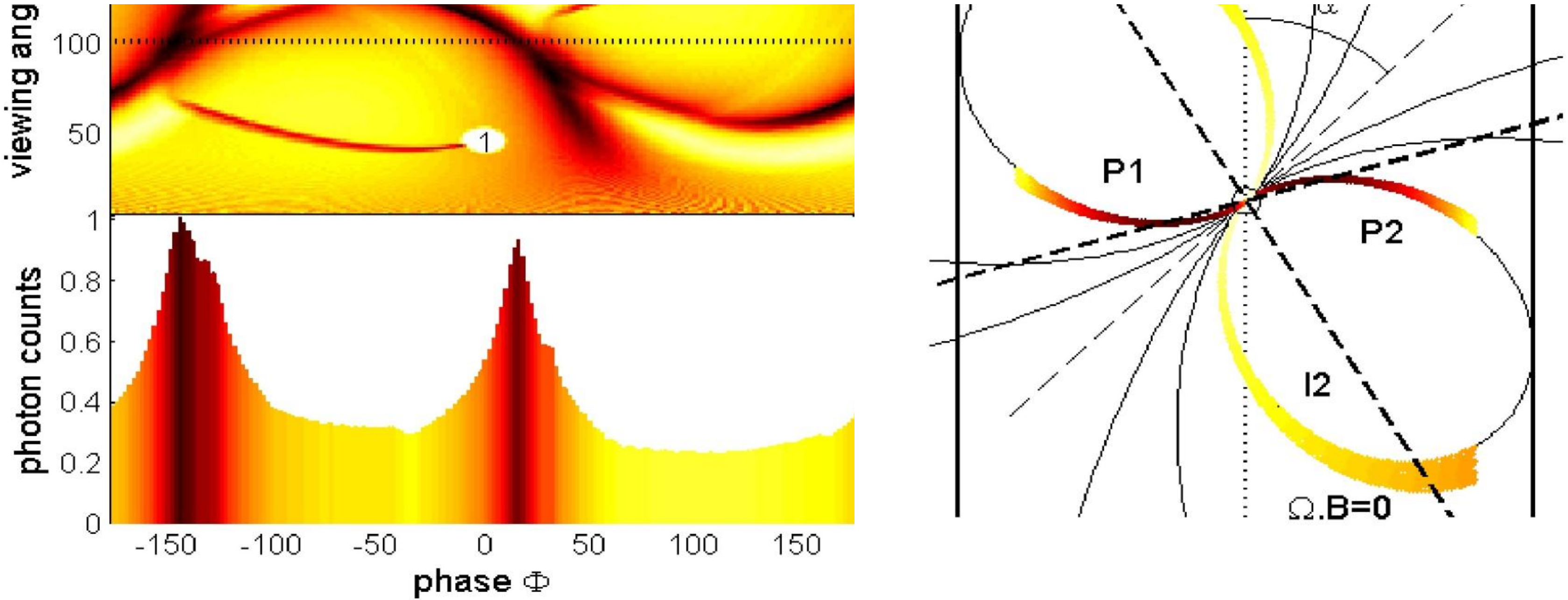

§3 Higher-altitude Pulsar Emission Models

Dyks, Harding, Rudak (2004, ApJ 606, 1125) showed that Crab pulsar's optical polarization characteristics can be qualitatively reproduced by their SG model.

Harding+ (2008, ApJ ApJ 680, 1378) examined Crab's γ-ray emission and found that the pulse profiles and the phase-resolved spectrum are qualitatively reproduced.

However, unfortunately, the higher-altitude SG model contains two fatal electro-dynamical inconsistencies.

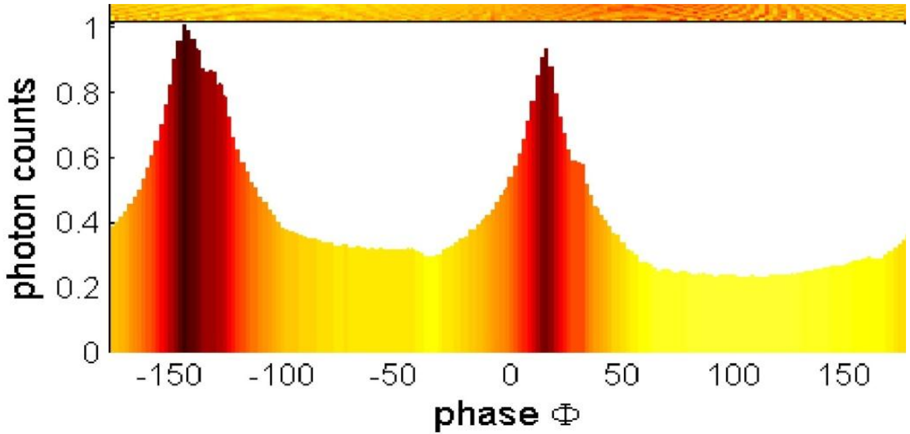

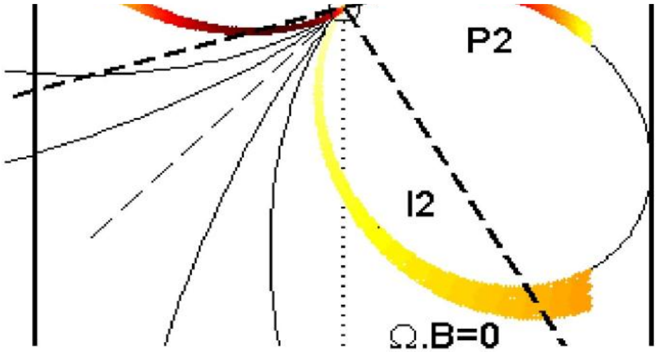

KH (2008) ApJ 688, L25

Problem 1: insufficient luminosity

Adopting the same parameter as Harding+(2008), one obtains too small γ-ray flux from a higher-altitude SG.

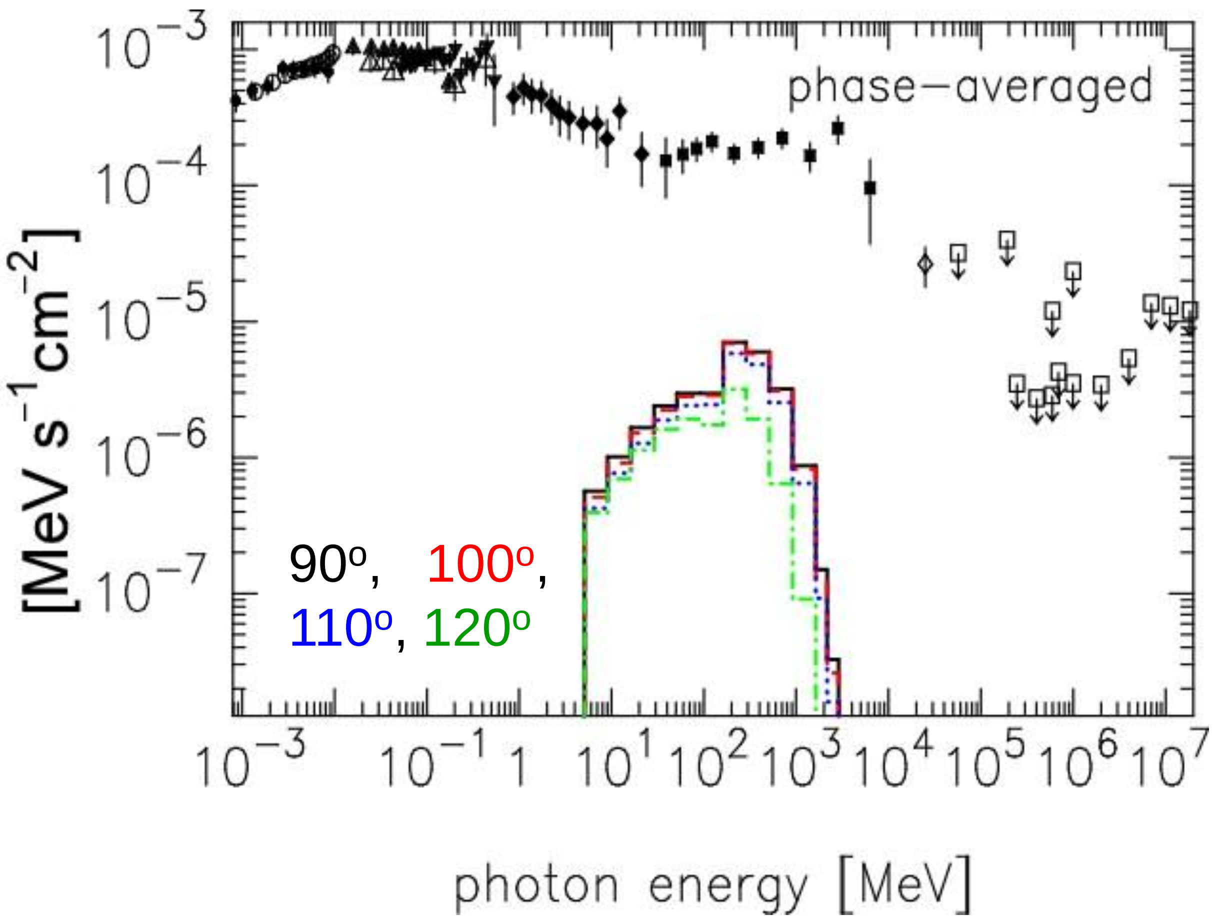

Fig. Phase-averaged SG spectrum for four discrete viewing angles, 90°, 100°, 110°, and 120°.

§4 Difficulties in SG Model: Insufficient Luminosity

Problem 1: insufficient luminosity

KH (2008) ApJ 688, L25

Adopting the same parameter as Harding+(2008), one obtains too small γ-ray flux from a higher-altitude SG.

Analytically predicted γ-ray flux of the Crab pulsar:

$$(\nu F_\nu)_{\rm peak} \approx 0.0450\, f^3 \kappa \underbrace{\frac{\mu^2\Omega^4}{c^3}\frac{1}{d^2}}_{\propto \dot{E}/d^2 \,:\ \text{spin-down flux}}, \qquad \kappa \sim 1.$$

f : fractional gap width ($f \ll 1$ denotes a thin gap)

The difference between OG and SG models appears through f, κ, and assumed μ (magnetic moment).

§4 Difficulties in SG Model: Insufficient Luminosity

Problem 1: insufficient luminosity

KH (2008) ApJ 688, L25

$$(\nu F_\nu)_{\rm peak} \approx 0.0450\, f^3 \kappa \frac{\mu^2 \Omega^4}{c^3} \frac{1}{d^2}$$

Apply this general result to the Crab pulsar (Ω=190 rad s^{-1}).

(I) For OG model (f~0.14, κ~0.3, μ=4×10^{30} G cm^3),

$(\nu F_\nu)_{\rm peak} \sim 4\times10^{-4}$ MeV s^{-1} cm^{-2} ~ EGRET flux.

(II) For SG model (f~0.04, κ~0.2), even with a large μ,

$(\nu F_\nu)_{\rm peak} \sim 3\times10^{-5}\,(\mu/8\times10^{30})^2$ MeV s^{-1} cm^{-2}
< 0.1 EGRET flux.

§4 Difficulties in SG Model: Insufficient Luminosity

Problem 1: insufficient luminosity

In short, both analytical and numerical results show that **a SG can produce a negligible γ-ray flux.**

(I) For OG model (f~0.14, κ~

$(\nu F_\nu)_{\rm peak}$ ~ 4×10^{-4} MeV

(II) For SG model (f~0.04, κ~

$(\nu F_\nu)_{\rm peak}$ ~ 3×10^{-5} (μ/8 ×

< 0.1 EGRET fl

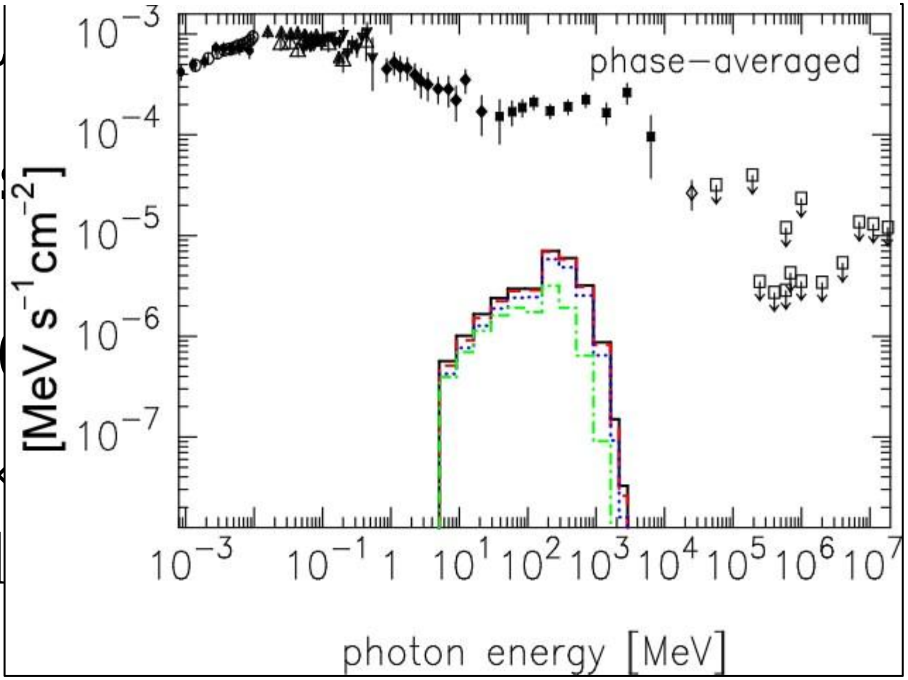

OG model remains as the only possible γ-ray pulsar model.

KH (2008) ApJ 688, L25

Problem 2: unphysical assumption of GJ charge density (per *B* flux tube)

Without pair creation, electron density per B will be constant along the field line. However, it results in a reversal of $E_{\parallel}$ due to the sign change of $\rho - \rho_{GJ}$.

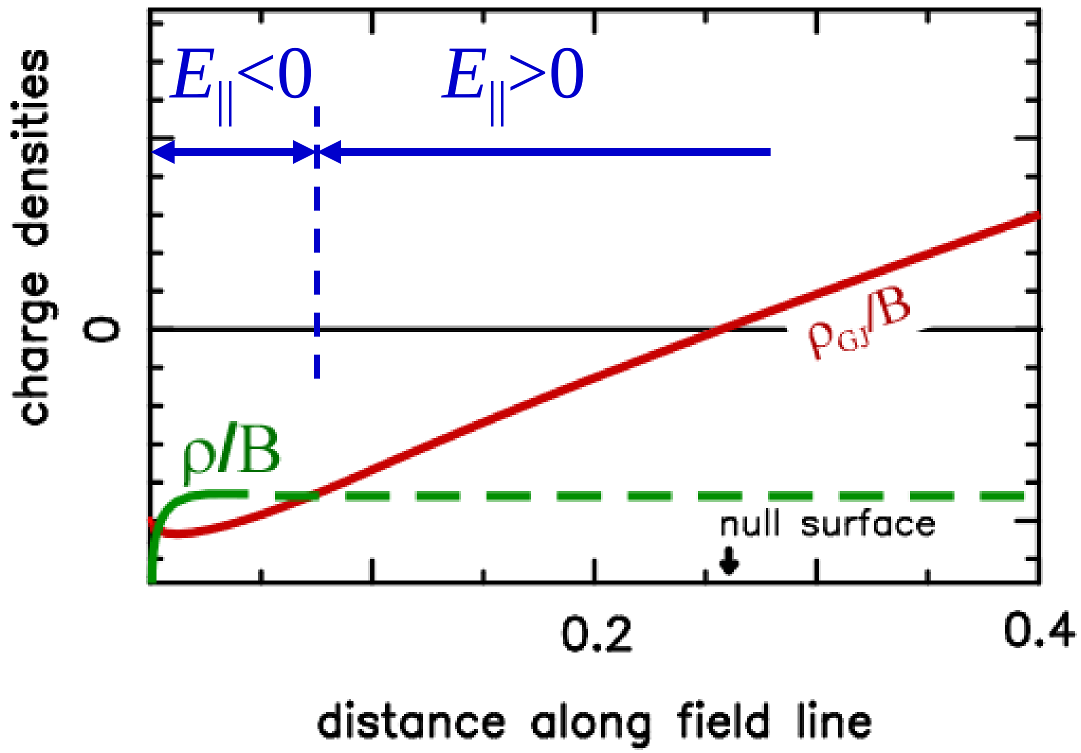

§5 Difficulties in SG Model: Unphysical GJ Charge

Problem 2: unphysical assumption of ρ_{GJ}/B

To prevent a sign reversal of $E_{\parallel}$, they assumed that ρ_{GJ}/B tends to a constant in the higher altitudes

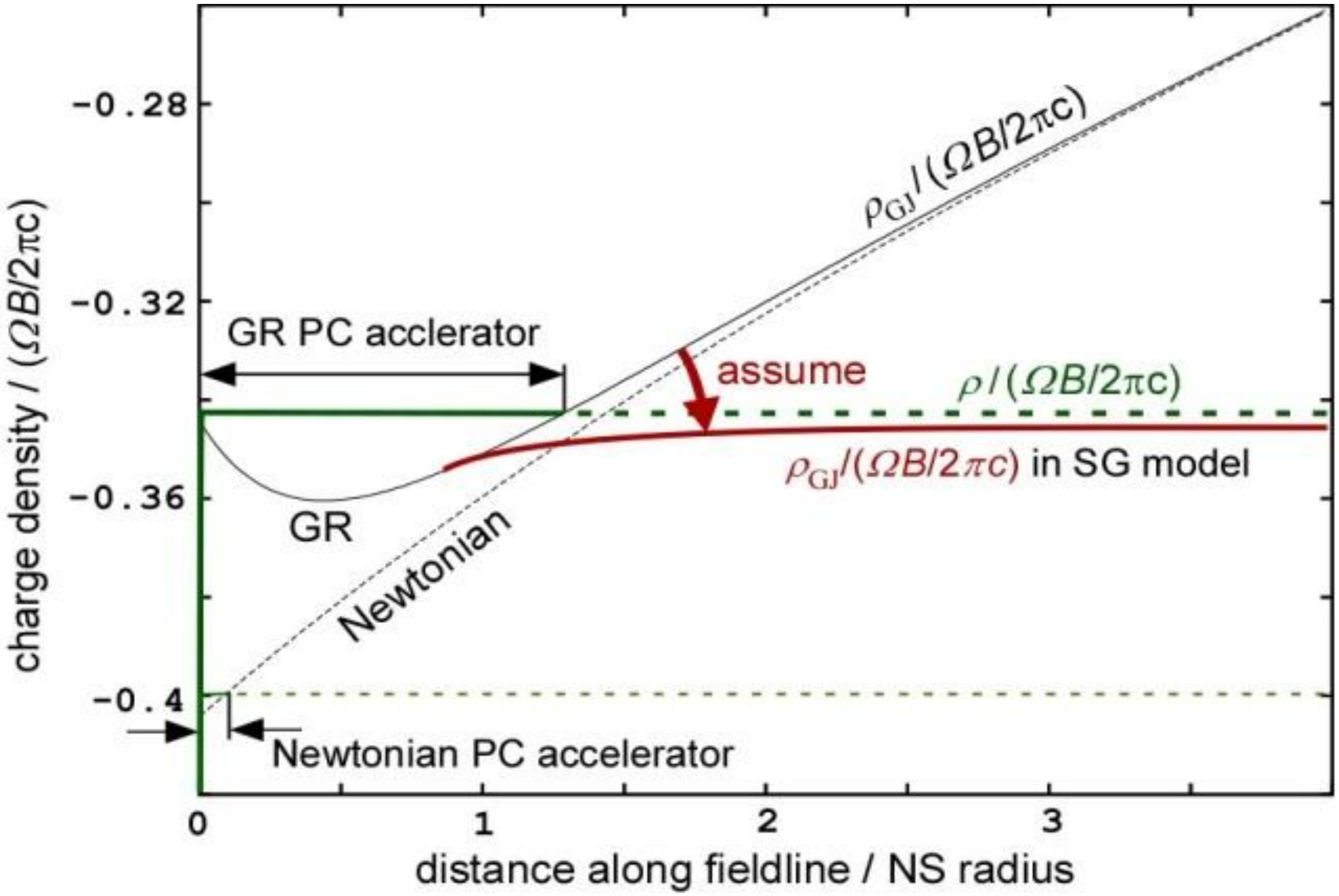

§5 Difficulties in SG Model: Unphysical GJ Charge

Problem 2: unphysical assumption of $\rho_{\mathrm{GJ}}/\mathrm{B}$

To prevent a sign reversal of $E_{\parallel}$, they assumed that $\rho_{\mathrm{GJ}}/\mathrm{B}$ tends to a constant in the higher altitudes.

However, Maxwell eq. uniquely gives

$$\rho_{\mathrm{GJ}} = \frac{c^2}{4\pi\sqrt{-g}}\partial_\mu\left(\frac{\sqrt{-g}}{\rho_w^2}g^{\mu\nu}g_{\varphi\varphi}(\Omega-\omega)F_{\varphi\nu}\right).$$

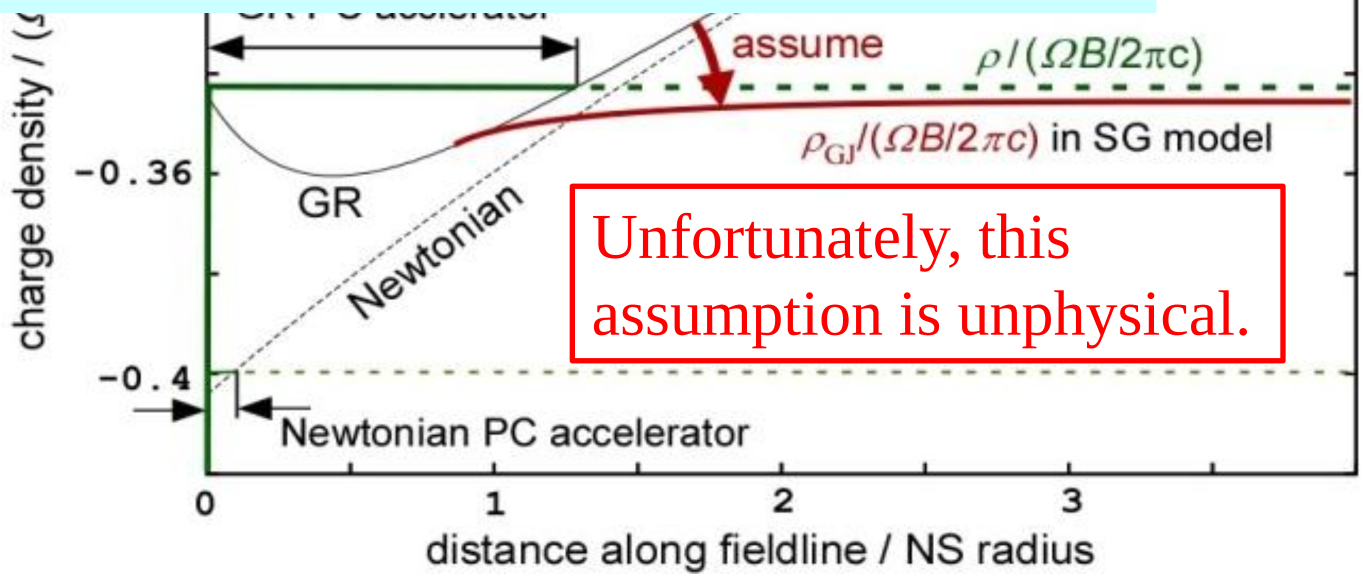

Unfortunately, this assumption is unphysical.

Problem 2: unphysical assumption of ρ_{GJ}/B

Since the pair-starved PC (PSPC) model adopts the same ρ_{GJ} distribution, this difficulty applies not only to the higher-altitude SG model, but also to the PSPC model (Venter+ 2009, ApJ 707, 800).

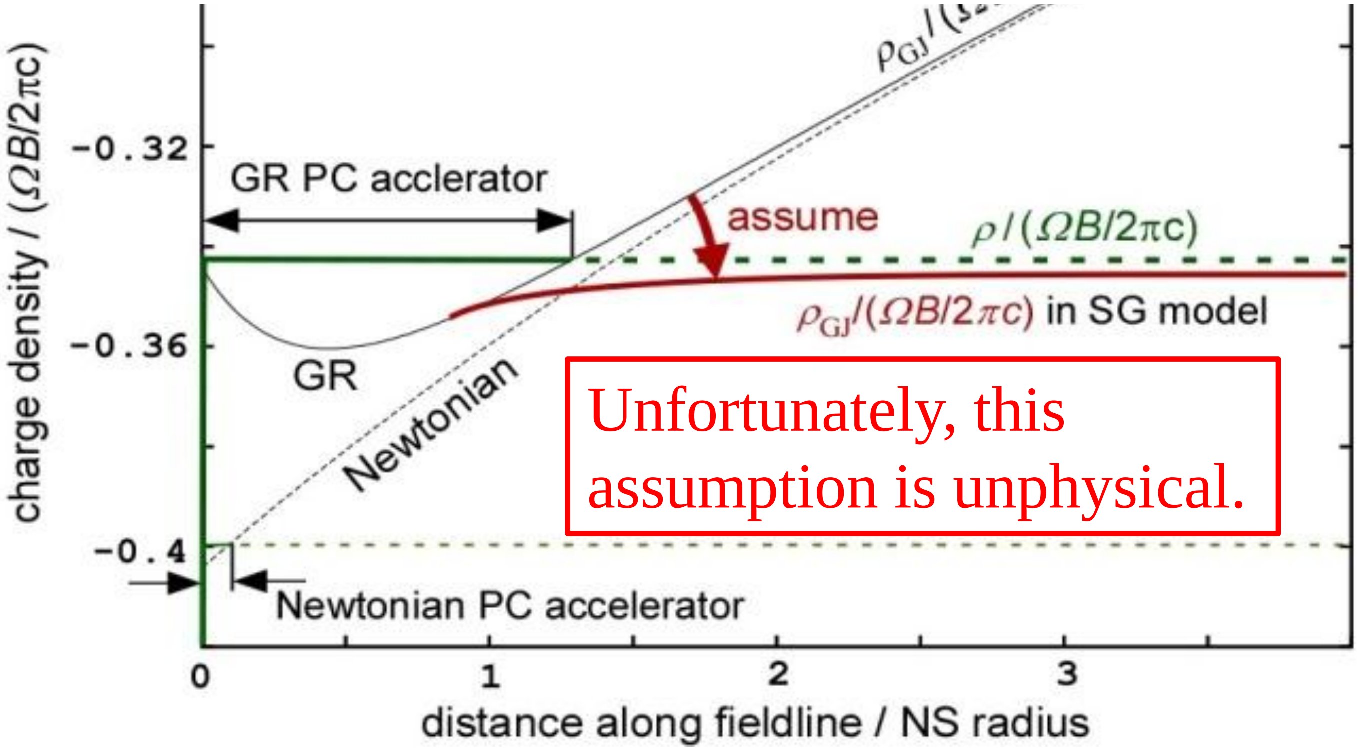

Problem 2: unphysical assumption of ρ_{GJ}/B

Since the pair-starved PC (PSPC) model adopts the same ρ_{GJ} distribution, this difficulty applies not only to the higher-altitude SG model, but also to the PSPC model (Venter+ 2009, ApJ 707, 800).

In short, higher-latitude SG model & PSPC model contain serious electro-dynamical problem that contradicts with Maxwell eq.

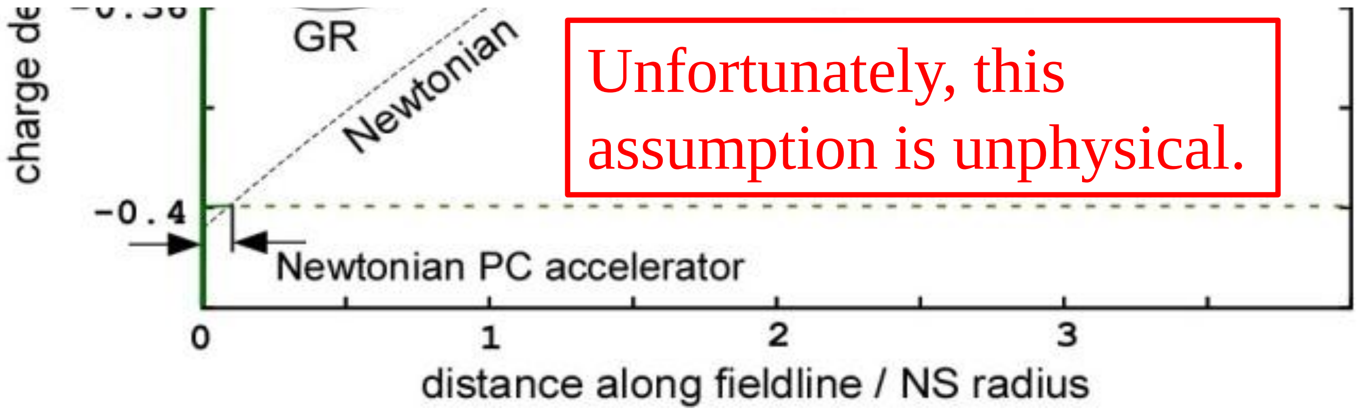

Unfortunately, this assumption is unphysical.

§6 Classic Outer-gap (OG) Models

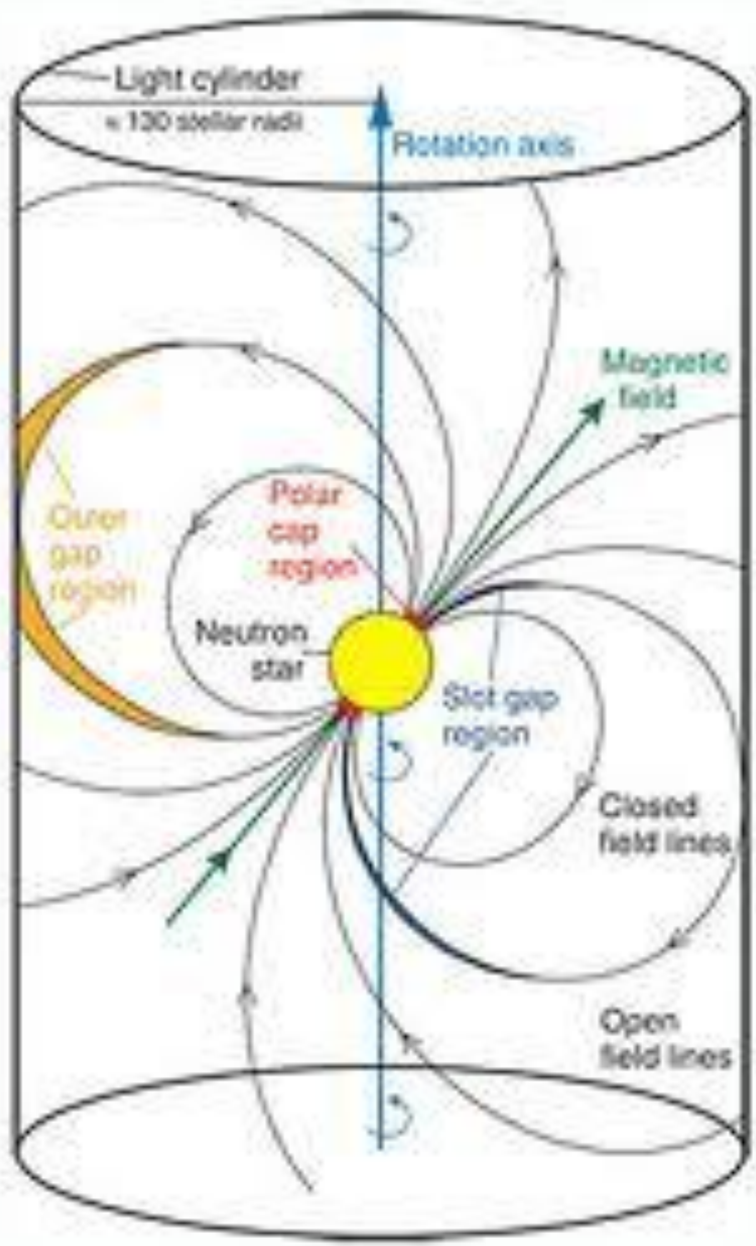

As an alternative possibility of high-altitude emission model, the outer gap model was proposed.

Cheng, Ho, Ruderman (1986, ApJ 300, 500)

So far, there have been found no serious electrodynamical problems in the OG model (unlike SG or PSPC model).

Thus, let us concentrate on the OG model in what follows.

§6 Classic OG Models

Mid 80's, the outer-gap (OG) model was proposed.

(Cheng, Ho, Ruderman ApJ 300, 500, 1986)

Emission altitude > 100 r_{NS} $\longrightarrow$ hollow cone emission

($\Delta\Omega > 1$ ster)

Mid 90s', OG model was further developed by including special relativistic effects. (Romani ApJ 470, 469)

$\longrightarrow$ Explains wide-separated double peaks.

Outer-gap model became promising.

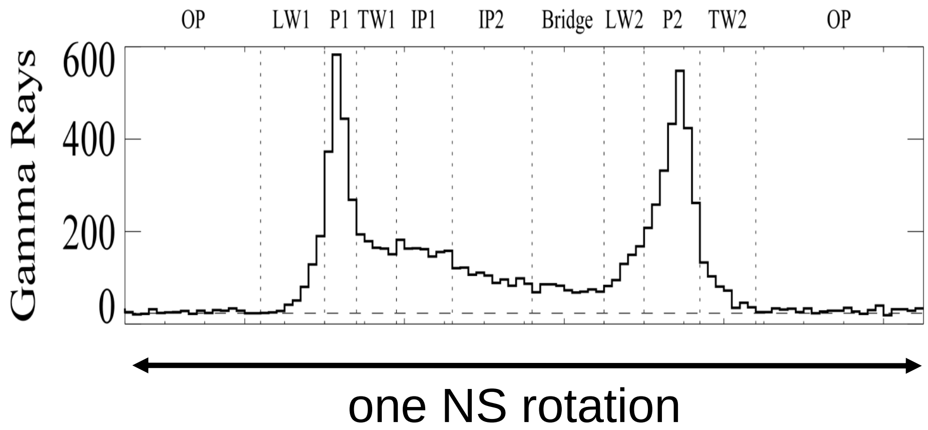

§6 Classic OG Models

Various attempts have been made on recent OG model:

3-D geometrical model

→ phase-resolved spectra (Cheng + '00; Tang + '08)

→ atlas of light curves for PC, OG, SG models

(Watters + '08)

2-D self-consistent solution (Takata + '06; KH '06)

3-D self-consistent solution

→ phase-resolved spectra, absolute luminosity

if we give only P, dP/dt, α, kT $(+\zeta)$ (this talk)

In this talk, I'll present the most recent results obtained in my 3-D version of self-consistent OG calculations.

§7 Modern Outer-gap Model

Self-sustained pair-production cascade in a rotating NS magnetosphere:

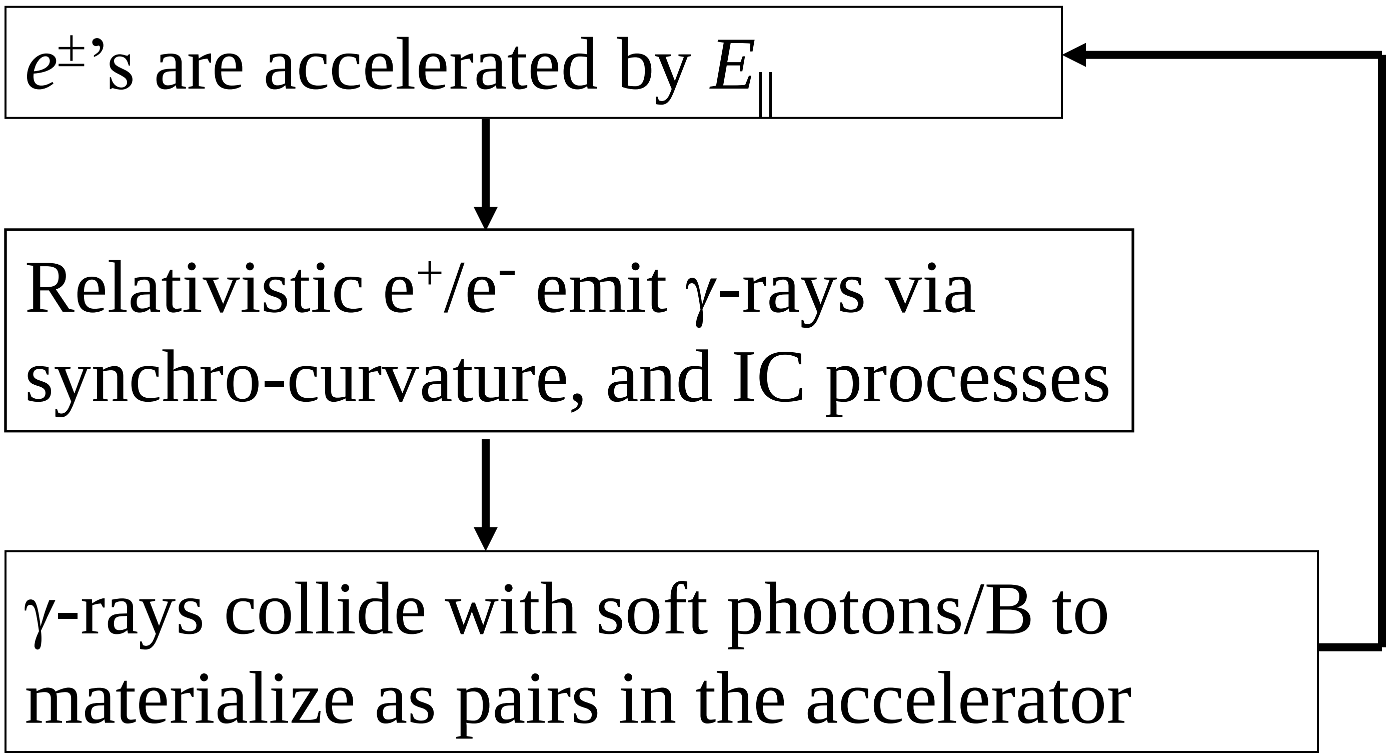

§7 Modern Outer-gap Model

The Poisson equation for the electrostatic potential ψ is given by

$$-\nabla^2\psi = 4\pi(\rho - \rho_{\rm GJ})\ ,$$

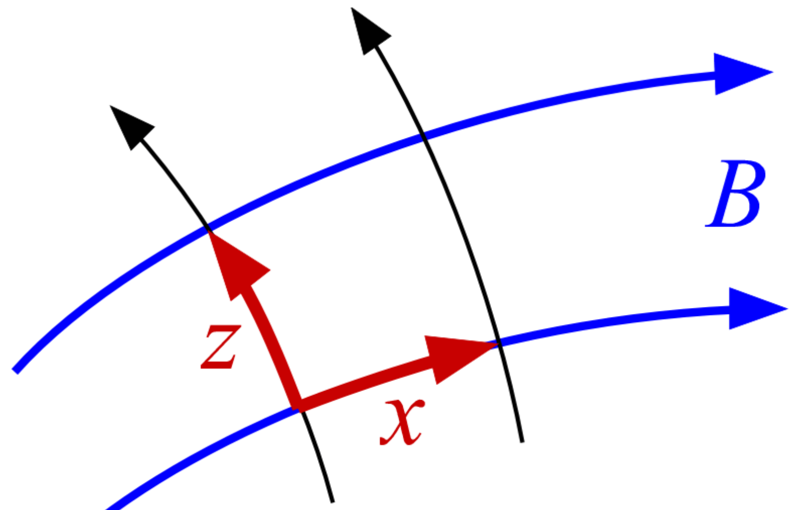

where

$$E_{\|} \equiv -\frac{\partial\Psi}{\partial x}\ ,\ \rho_{\rm GJ} \equiv -\frac{\mathbf{\Omega}\bullet\mathbf{B}}{2\pi c},$$

$$\rho \equiv e\int_0^\infty d\mathbf{p}^3\left[N_+(\mathbf{x},\mathbf{p}) - N_-(\mathbf{x},\mathbf{p})\right] + \rho_{\rm ion}\ .$$

N_+/N_-: distrib. func. of e^+/e^-

$\boldsymbol{p}$: momentum of e^+/e^-

§7 Modern Outer-gap Model

Assuming $\partial_t + \Omega\partial_\phi = 0$, we solve the $e^{\pm}$'s Boltzmann eqs.

$$\frac{\partial N_\pm}{\partial t} + \vec{v}\cdot\nabla N_\pm + \left(e\vec{E}_\parallel + \frac{\vec{v}}{c}\times\vec{B} \right)\cdot\frac{\partial N_\pm}{\partial \vec{p}} = S_{IC} + S_{SC} + \int \alpha_\nu d\nu \int \frac{I_\nu}{h\nu} d\omega$$

together with the radiative transfer equation,

$$\frac{dI_\nu}{dl} = -\alpha_\nu I_\nu + j_\nu$$

$N_\pm$: positronic/electronic spatial # density,

$E_\parallel$: mangnetic-field-aligned electric field,

S_{IC}: ICS re-distribution function, $d\omega$: solid angle element,

I_ν: specific intensity, l : path length along the ray

α_ν: absorption coefficient, j_ν: emission coefficient

§7 Modern Outer-gap Model

Specify the three parameters: (period P is known)

- magnetic inclination (e.g., $\alpha_{\rm inc}$=45°, 75°),
- magnetic dipole moment of NS (e.g., $\mu=4\times10^{30}\,{\rm G\,cm^3}$)
- neutron-star surface temperature (e.g., $kT_{\rm NS}$=50 eV)

Solve Poisson eq. + Boltzmann eqs + radiative transf. eq.

I first solved (in 6-D phase space)

- 3-D gap geometry,
- acceleration electric field distribution, $E_{\parallel}$,
- particle density and energy spectrum,
- photon specific intensity (→predicts γ-ray properties),

by specifying these three parameters, assuming ***B***-field structure by vacuum rotating dipole solution (Cheng + '00).

§8 ICS spectrum of the Crab pulsar

Let us apply this numerical method to the Crab pulsar.

Maxwell & Boltzmann eqs., ⇒

- OG 3-D geometry,
- $E_{||}$ distribution,
- e^+/e^- distribution functions,
- photon specific intensity

Apply this method to the Crab pulsar, assuming

μ=3.8 × 10^{30} G cm^3, α=60^o , kT= 100 eV.

3-D distribution of the particle accelerator (i.e., high-energy emission zone) solved from the Poisson eq.:

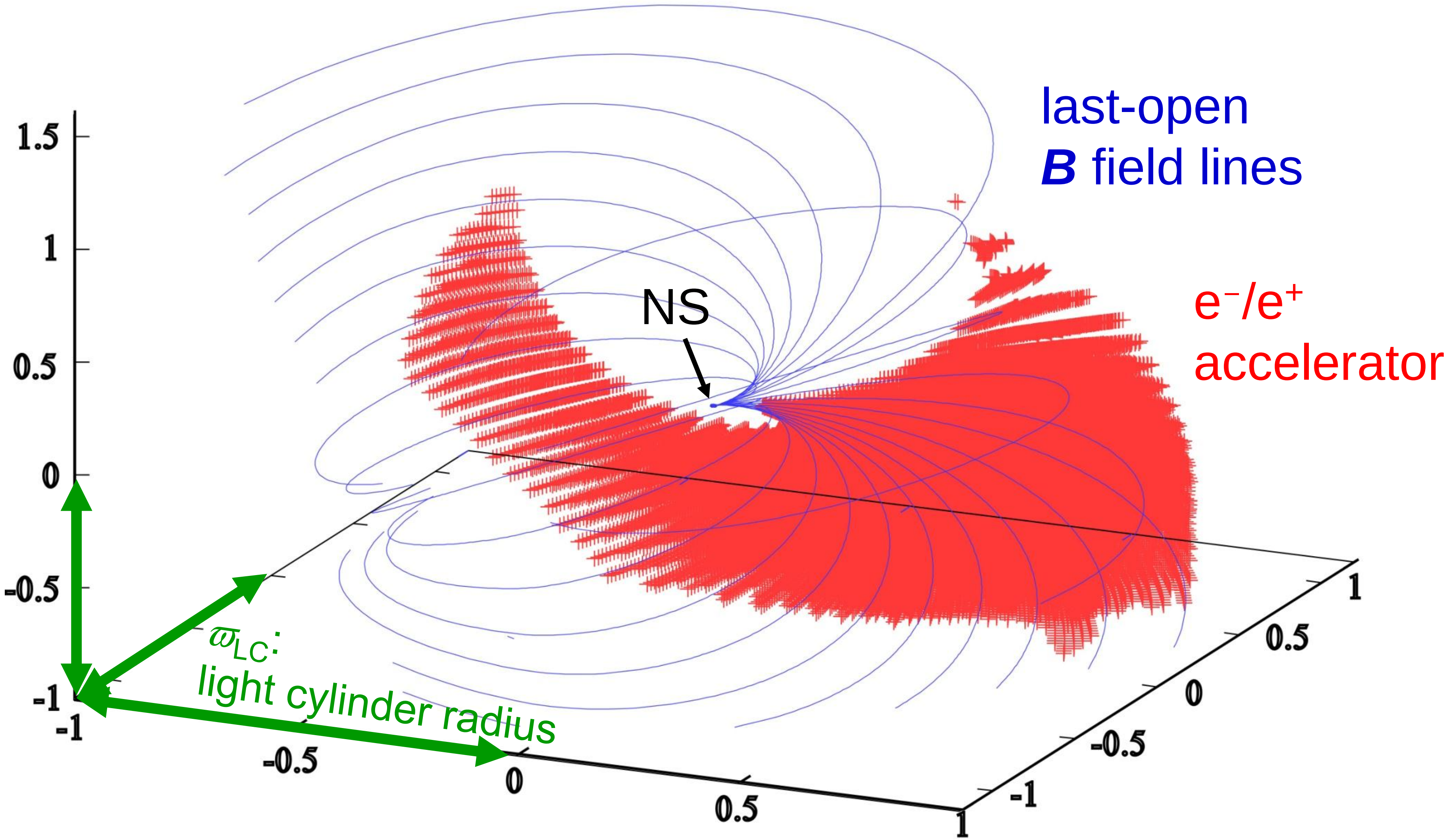

3-D geometry: Trans-field gap thickness is self-regulated by pair production.

Crab, α=60°

Fractional gap thickness projection on the last-open ***B*** line surface

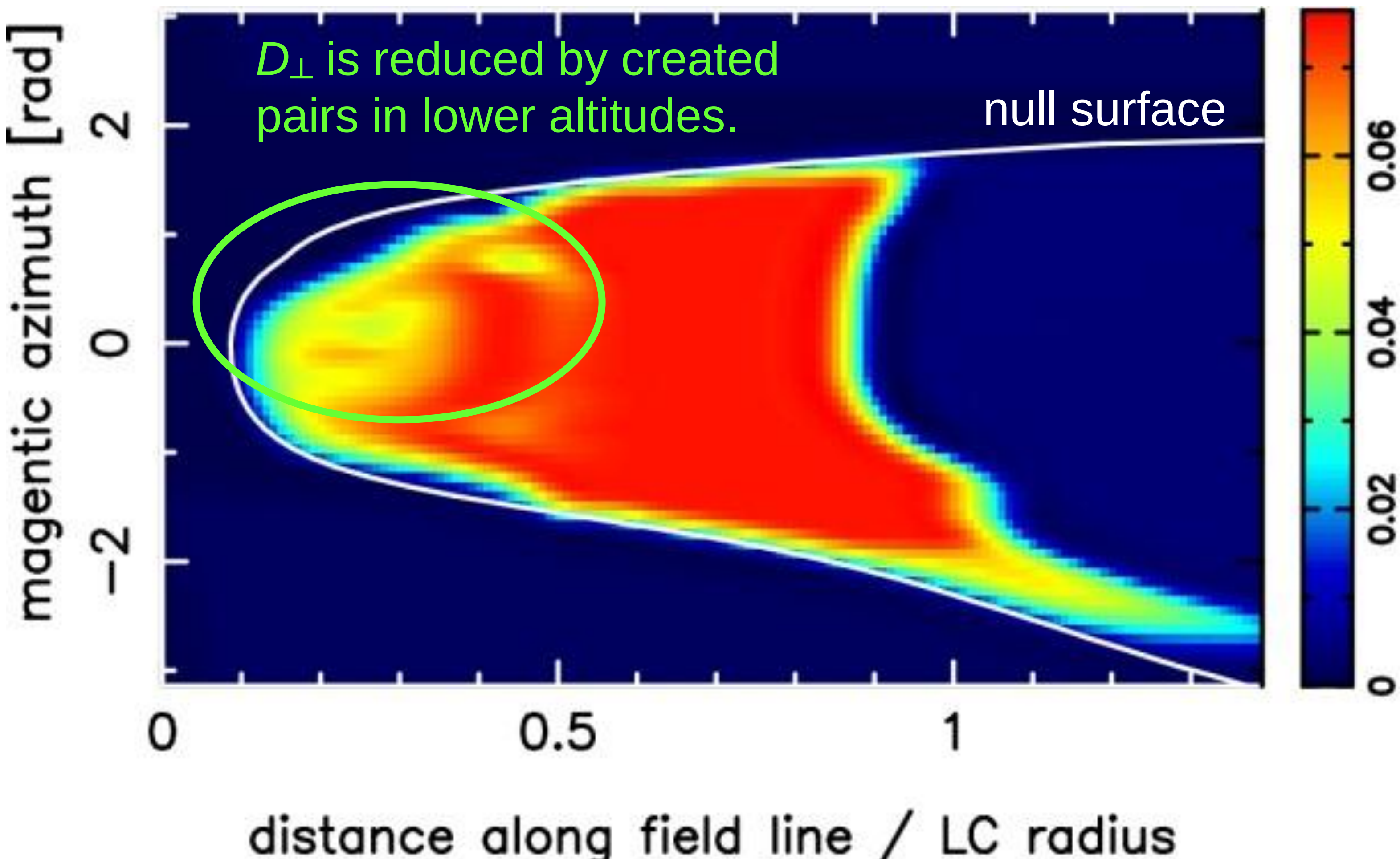

$E_{||}$ is also self-regulated by pair production.
(→ Curvature photon energy changes little for various pulsars.)

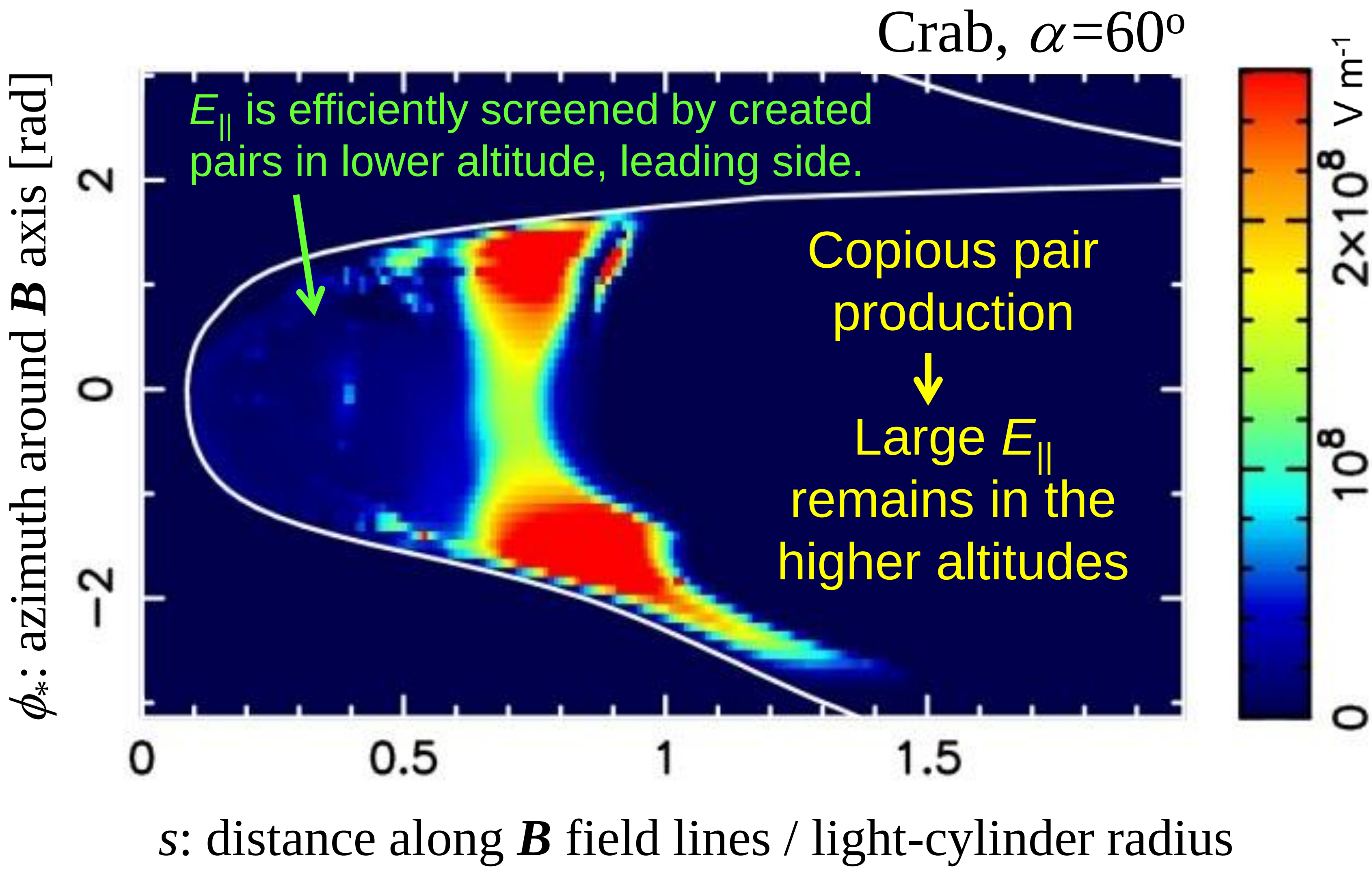

$E_\parallel$ is also self-regulated by pair production.

(→ Curvature photon energy changes little for various pulsars.)

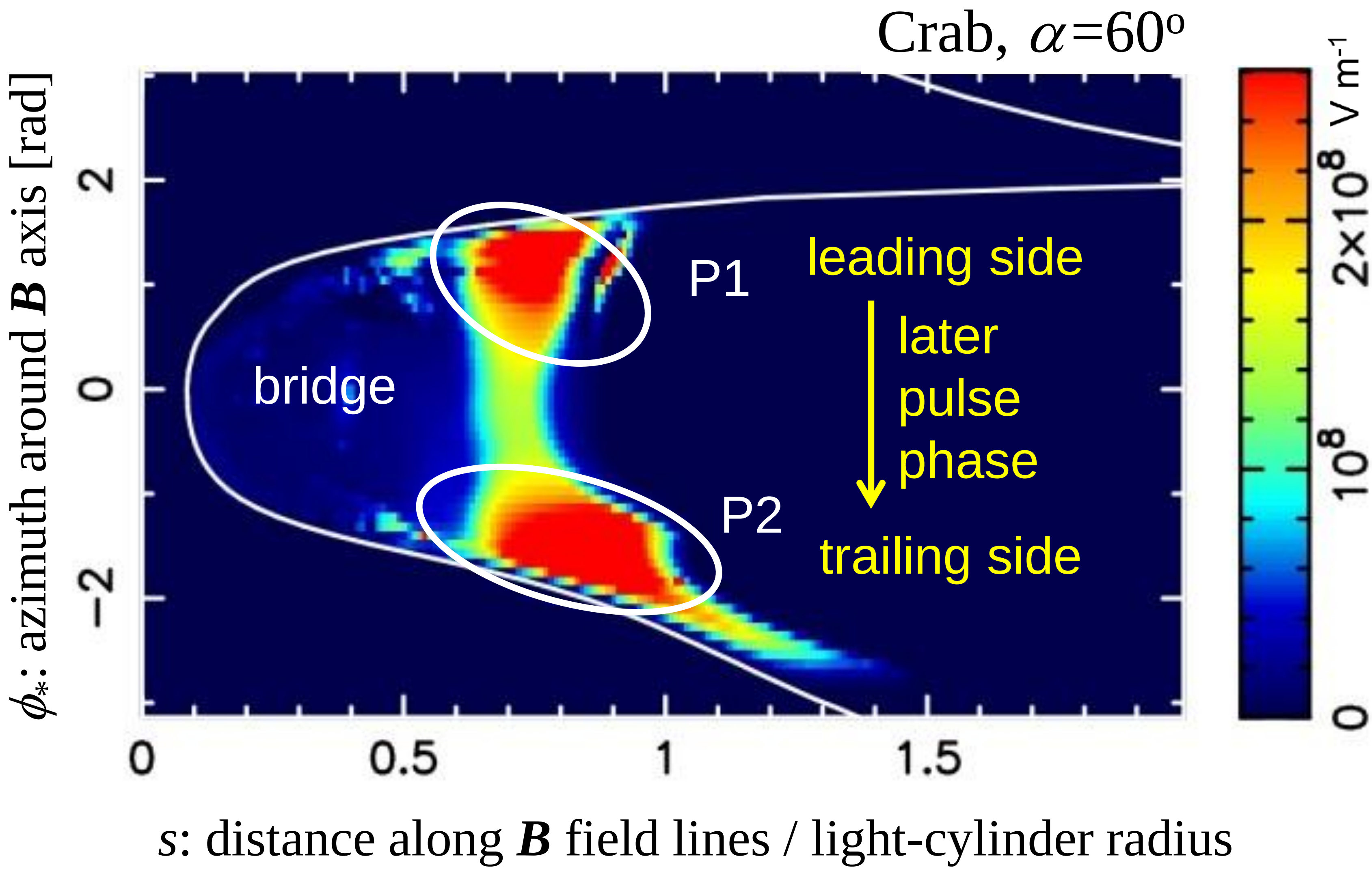

§8 HE/VHE Pulsation from the Crab Pulsar

Crab 60°

Using $E_{||}$, compute emissivity at each position.

Intensity distribution shows caustic pattern in the sky map.

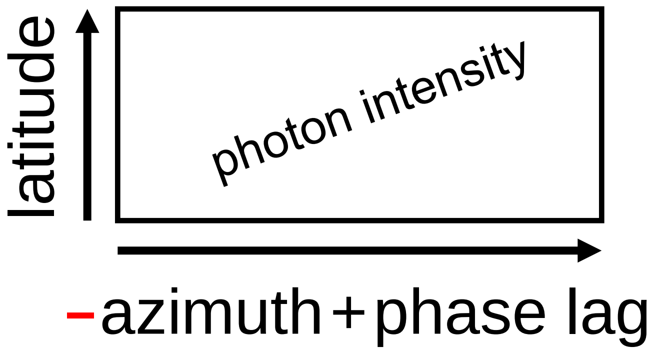

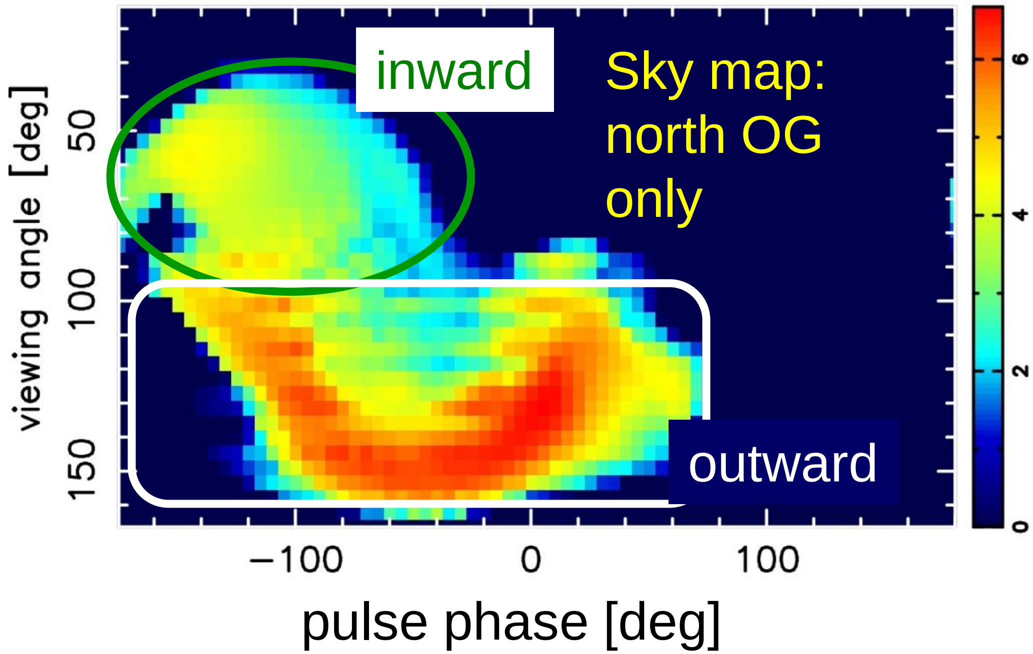

one NS rotation

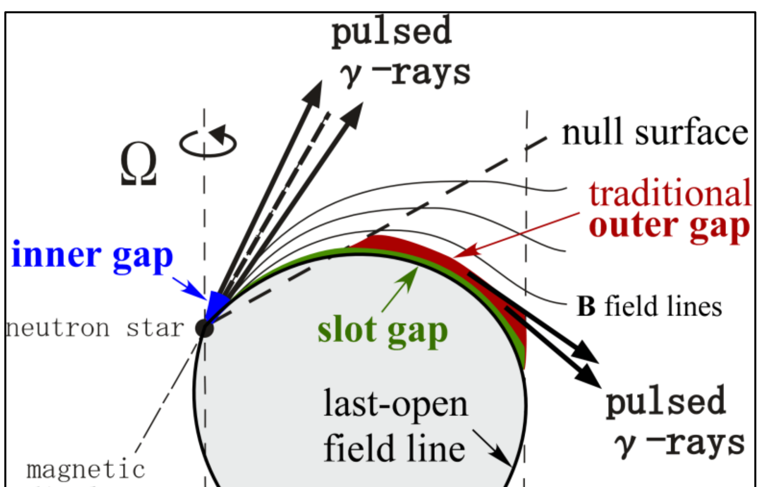

§8 HE/VHE Pulsation from the Crab Pulsar

Crab 60°

Using $E_{||}$, compute emissivity at each position.

Intensity distribution shows caustic pattern in the sky map.

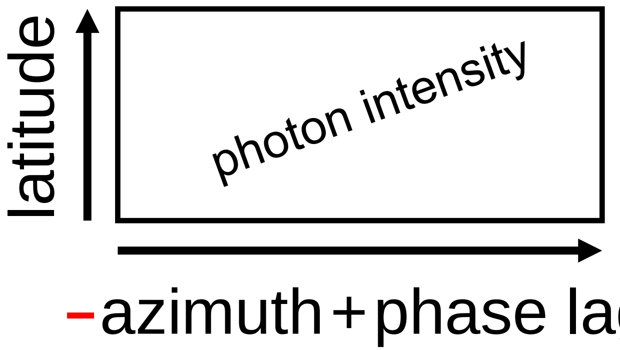

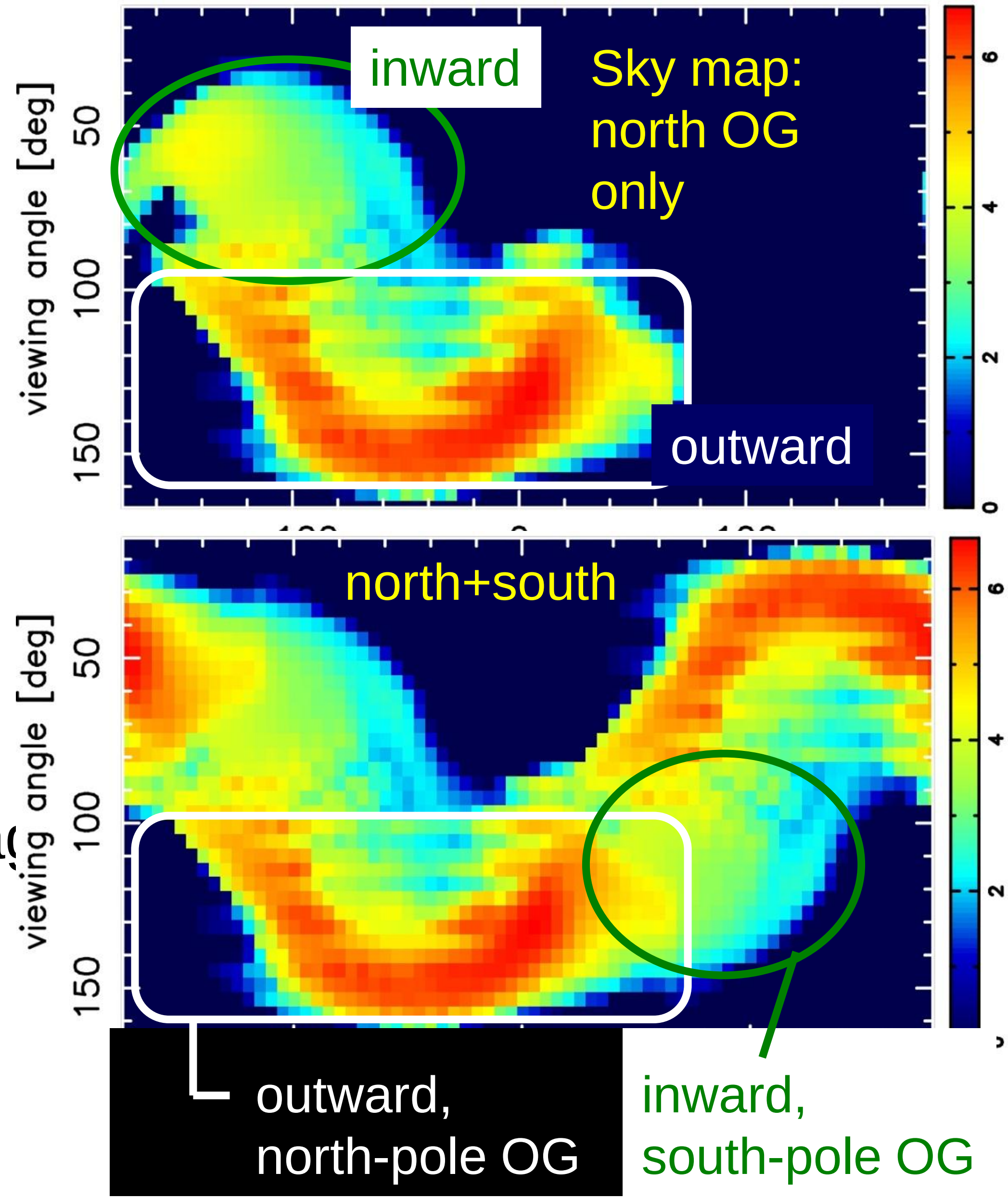

Consider photons emitted from OGs connected to **both poles**.

§8 HE/VHE Pulsation from the Crab Pulsar

Crab 60^o

Cut the sky map at a viewing angle ζ to obtain a pulse profile.

With energy-dependent sky map, we obtain pulse profiles at different energies.

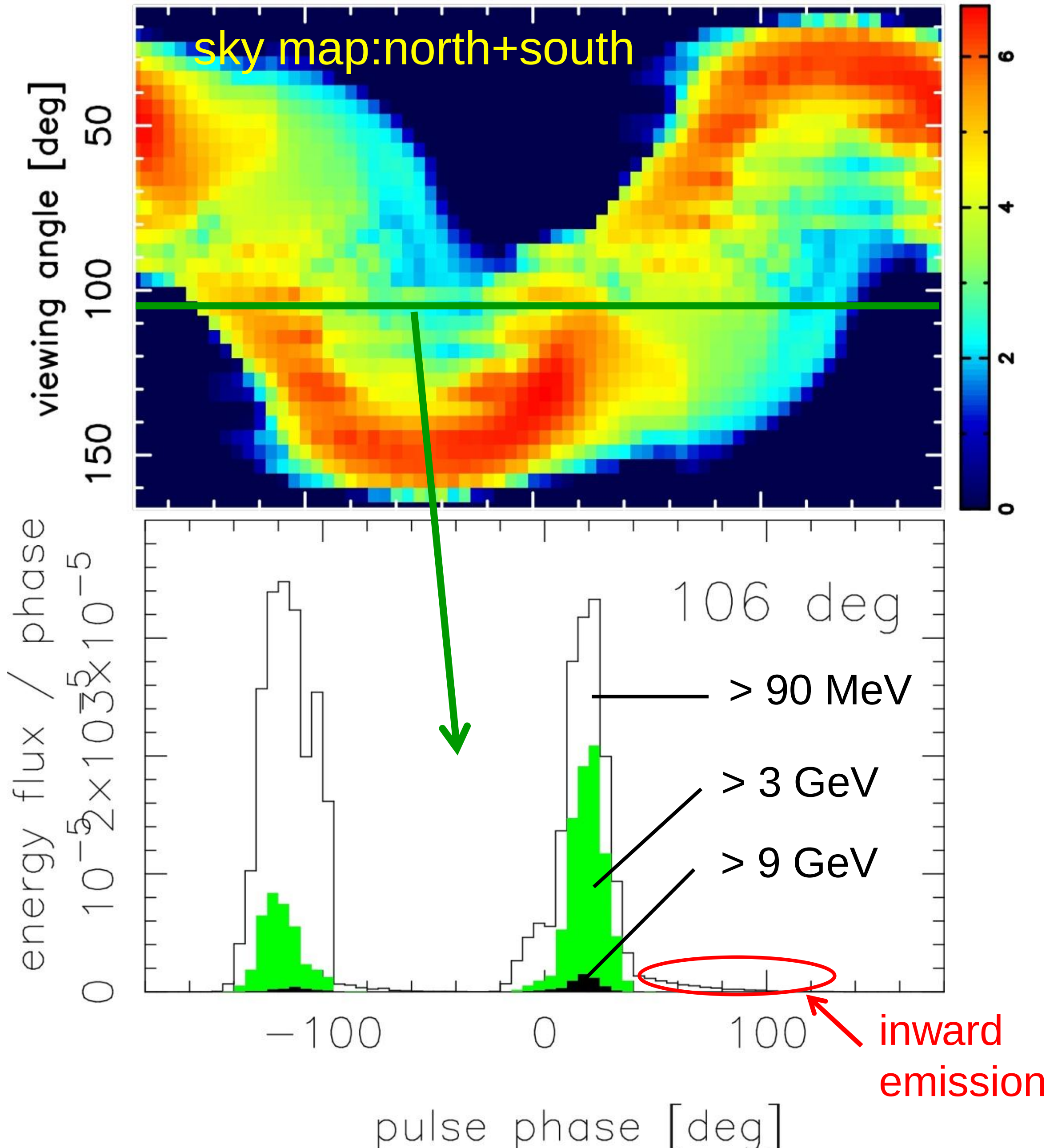

§8 HE/VH

If we look at the details, however, the energy-dependent pulse profile does not reproduce the Fermi and MAGIC observations.

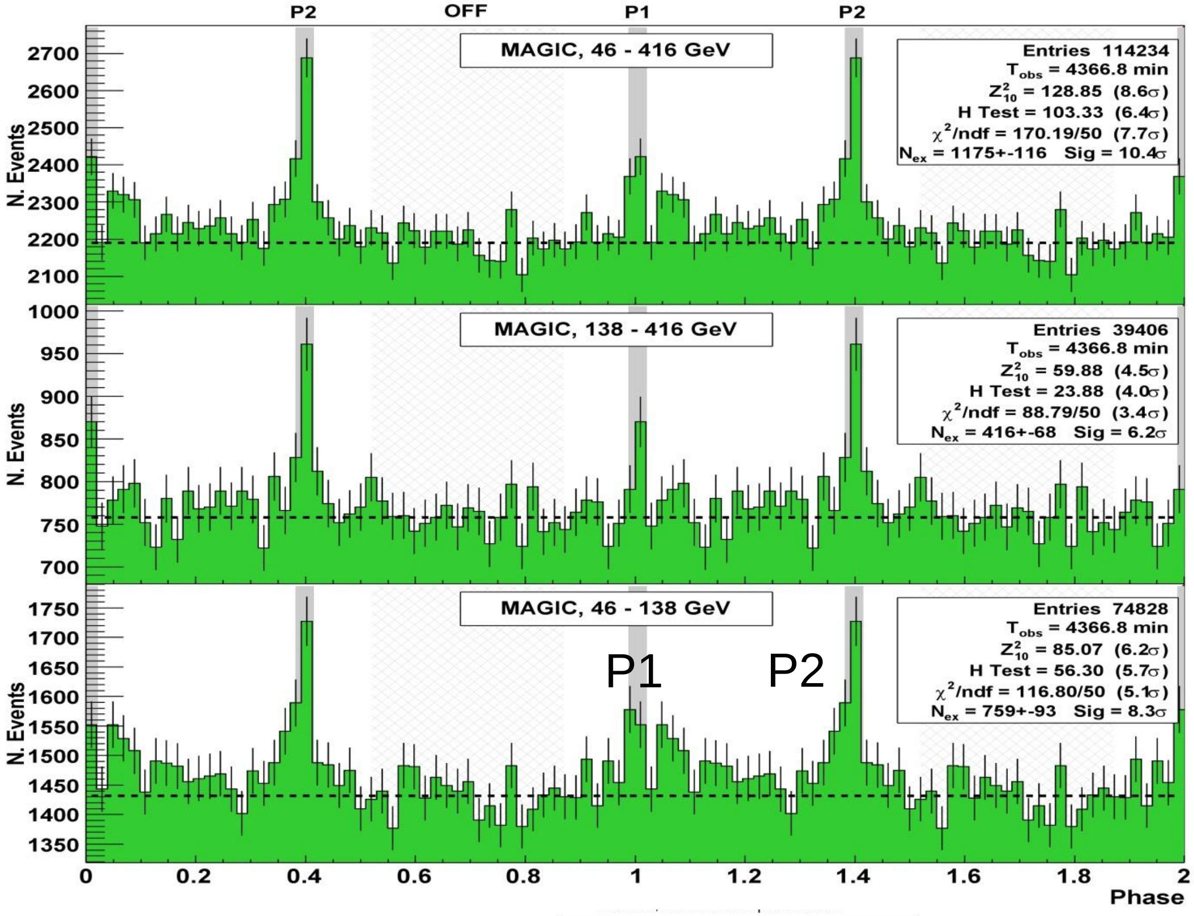

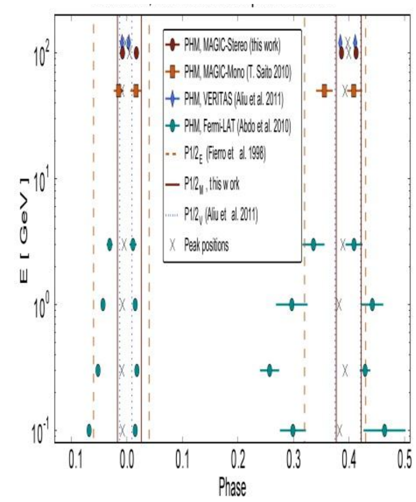

higher energies

§8 HE/VHE Pulsation from the Crab Pulsar

Some details …

The peak width appears to be roughly constant from 0.1 to 10 GeV, while observed peak width sharpens in higher energies.

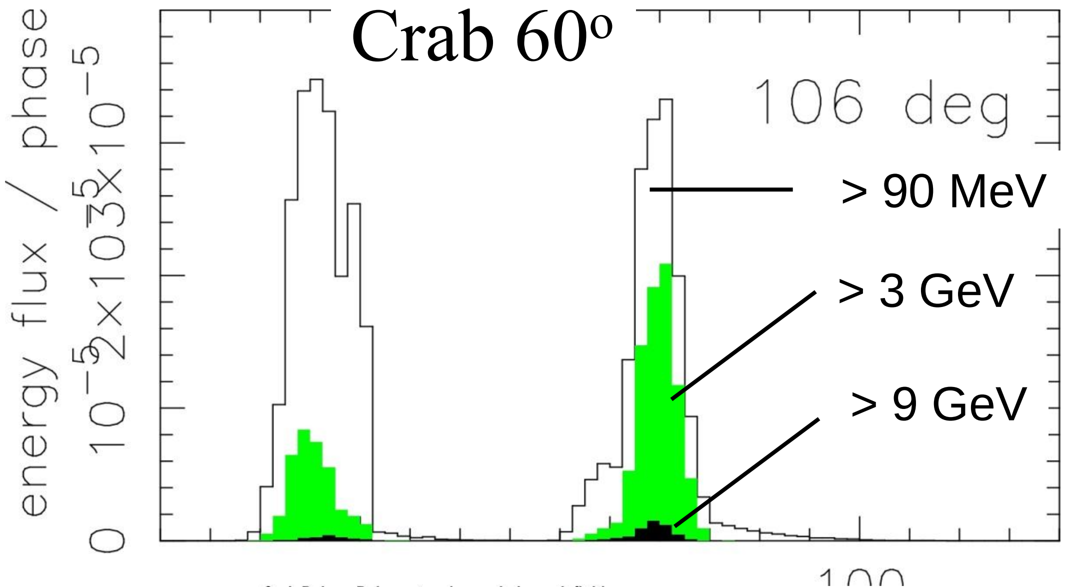

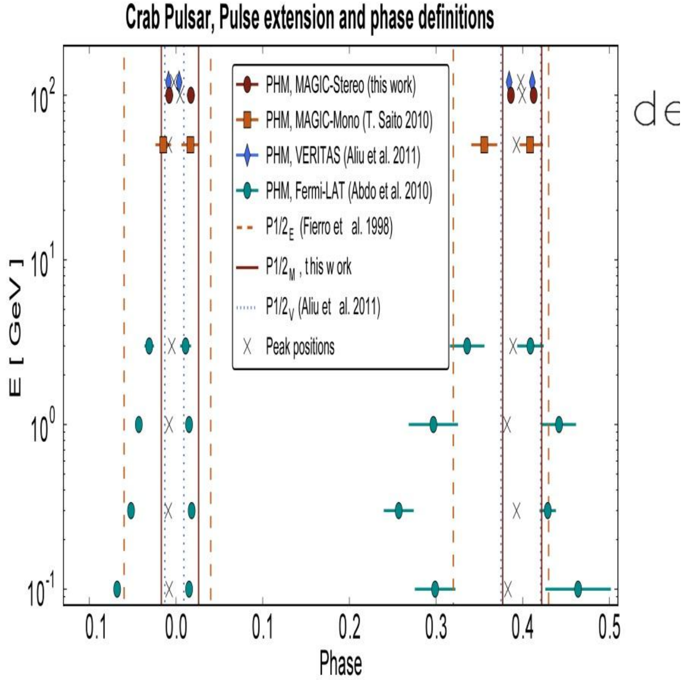

§8 HE/VHE Pulsation from the Crab Pulsar

Phase-averaged spectrum

solid: primary (bef. absorption)
dashed: secondary (bef. absorption)
dotted: tertiary (bef. absorption)
green: all (after absorption)

Crab, α=60°

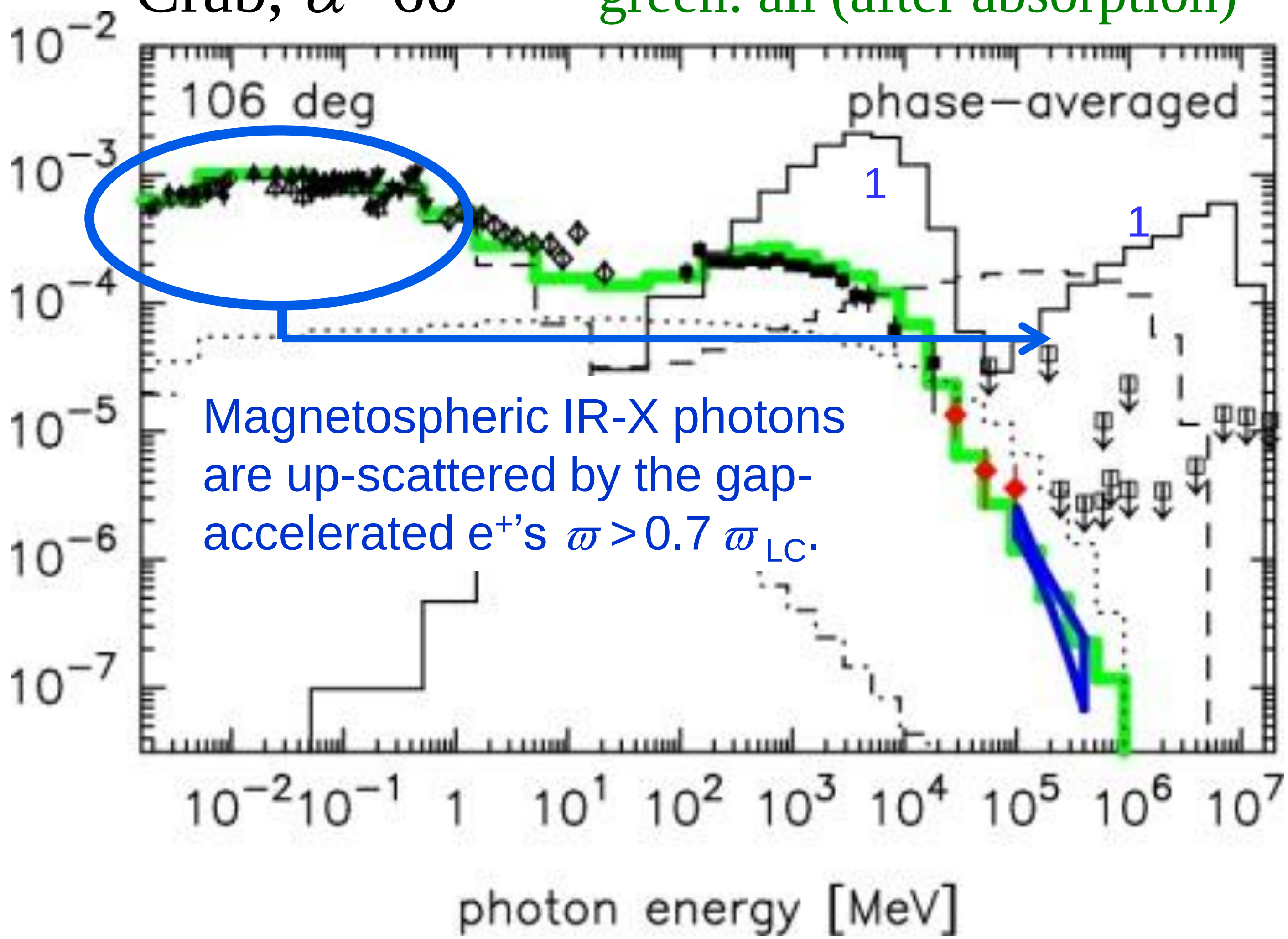

Phase-averaged spectrum

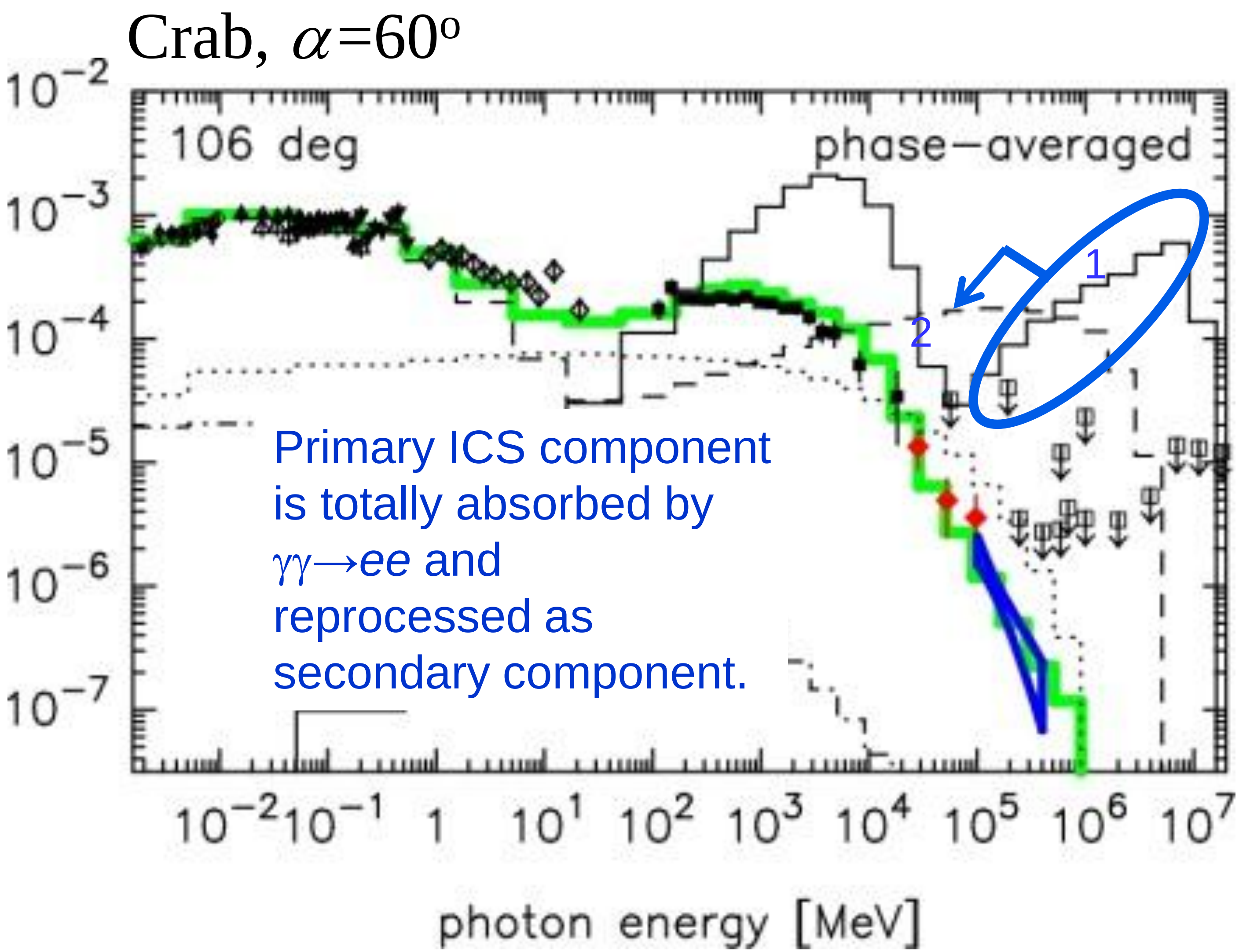

Phase-averaged spectrum

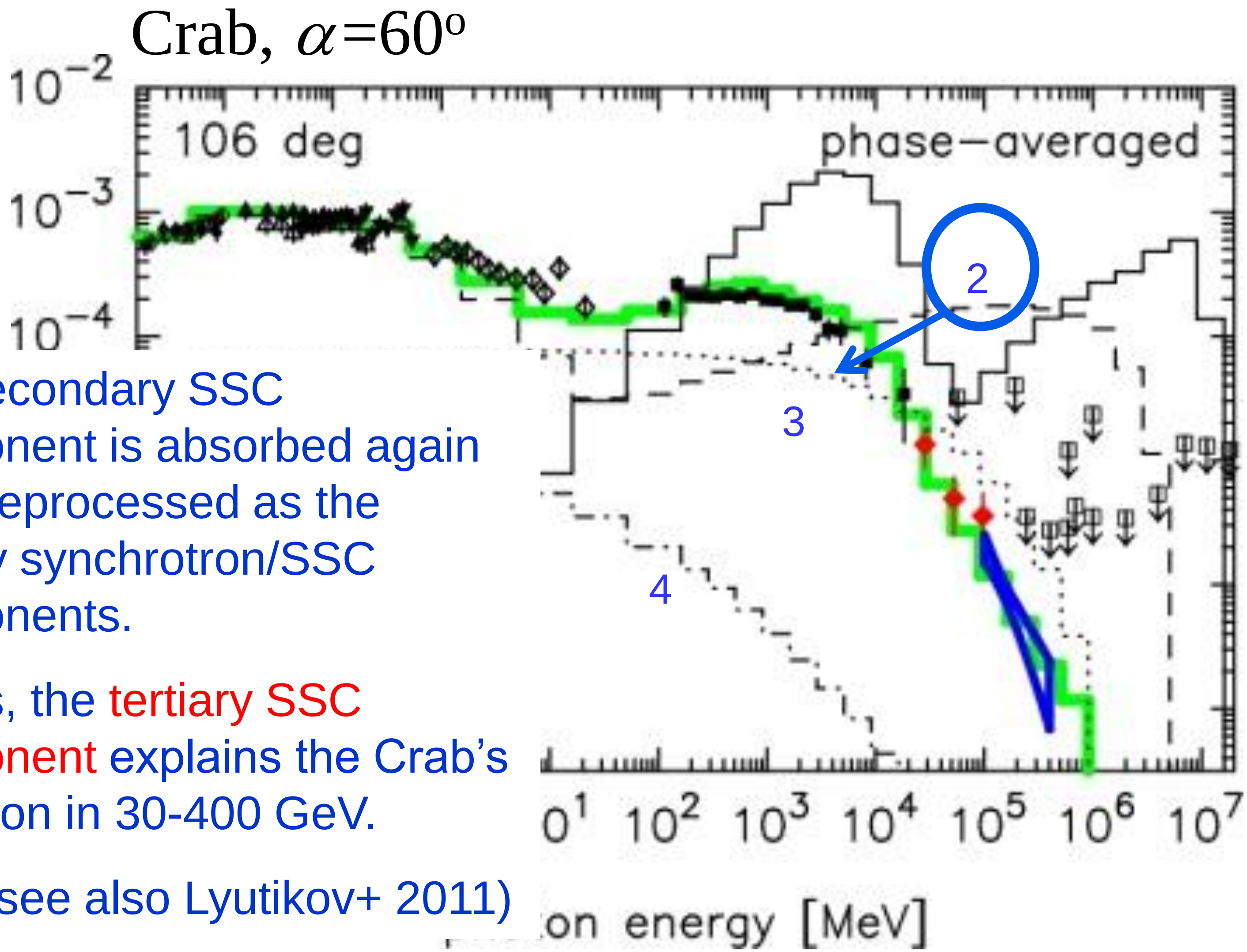

The secondary SSC component is absorbed again to be reprocessed as the tertiary synchrotron/SSC components.

That is, the tertiary SSC component explains the Crab's pulsation in 30-400 GeV.

(see also Lyutikov+ 2011)

§8 HE/VHE Pulsation from the Crab Pulsar

Phase-resolved spectrum (in LAT-defined phase bins):

Crab, α=60°

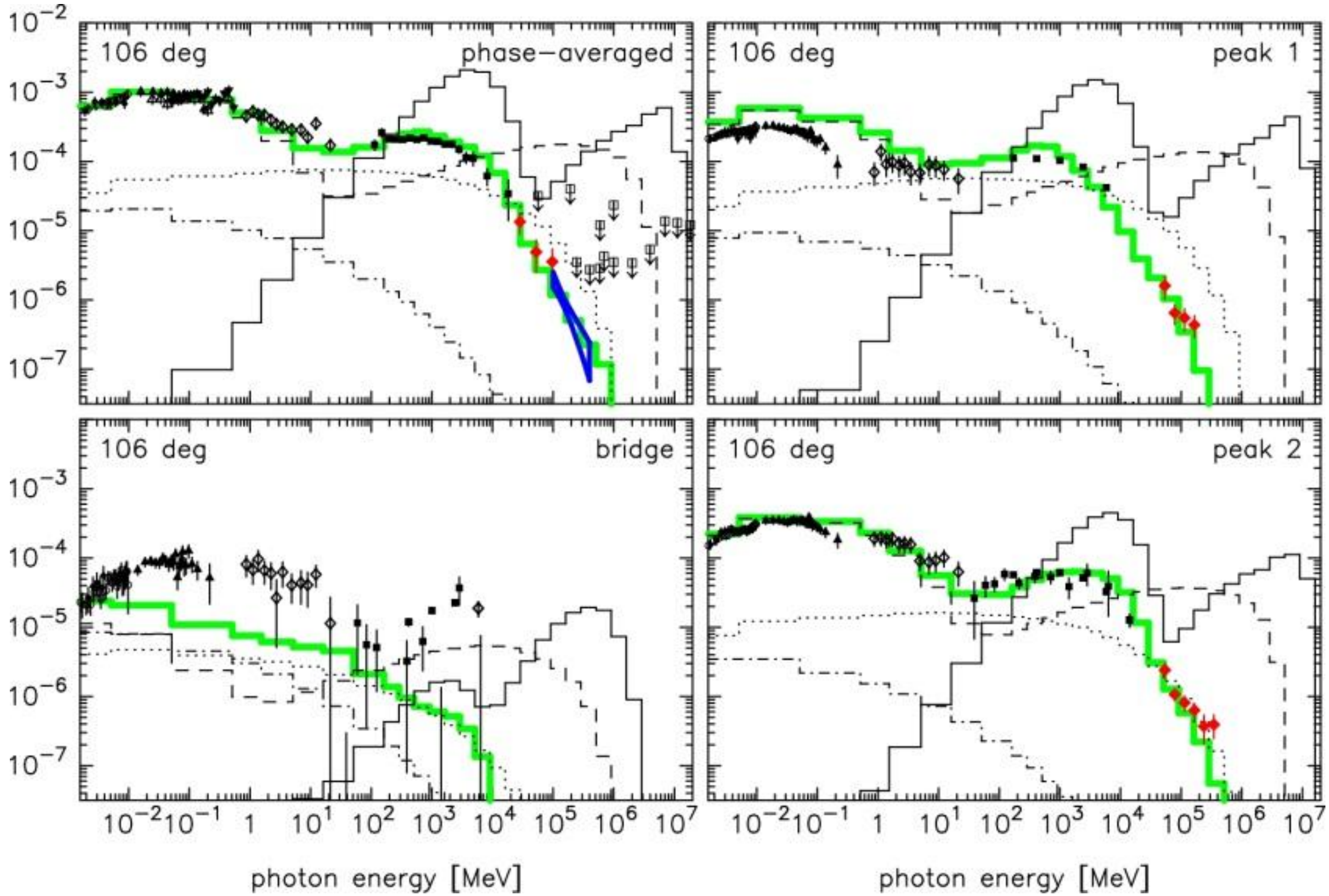

Phase-resolved spectrum (in LAT-defined phase bins):

Crab, α=60°

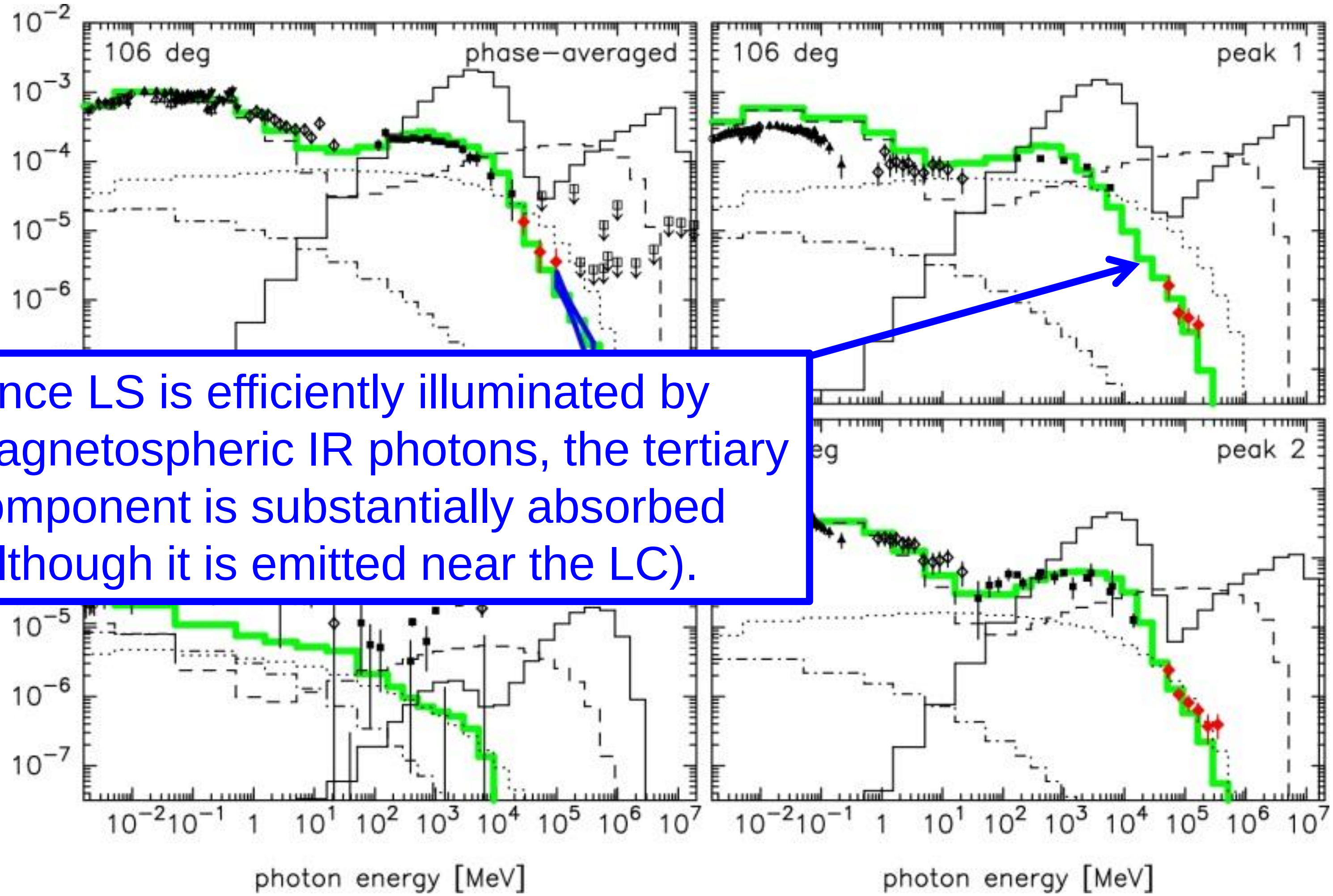

Since LS is efficiently illuminated by magnetospheric IR photons, the tertiary component is substantially absorbed (although it is emitted near the LC).

Viewing angle dependence of phase-averaged spectrum:

Crab, $\alpha=60^{o}$

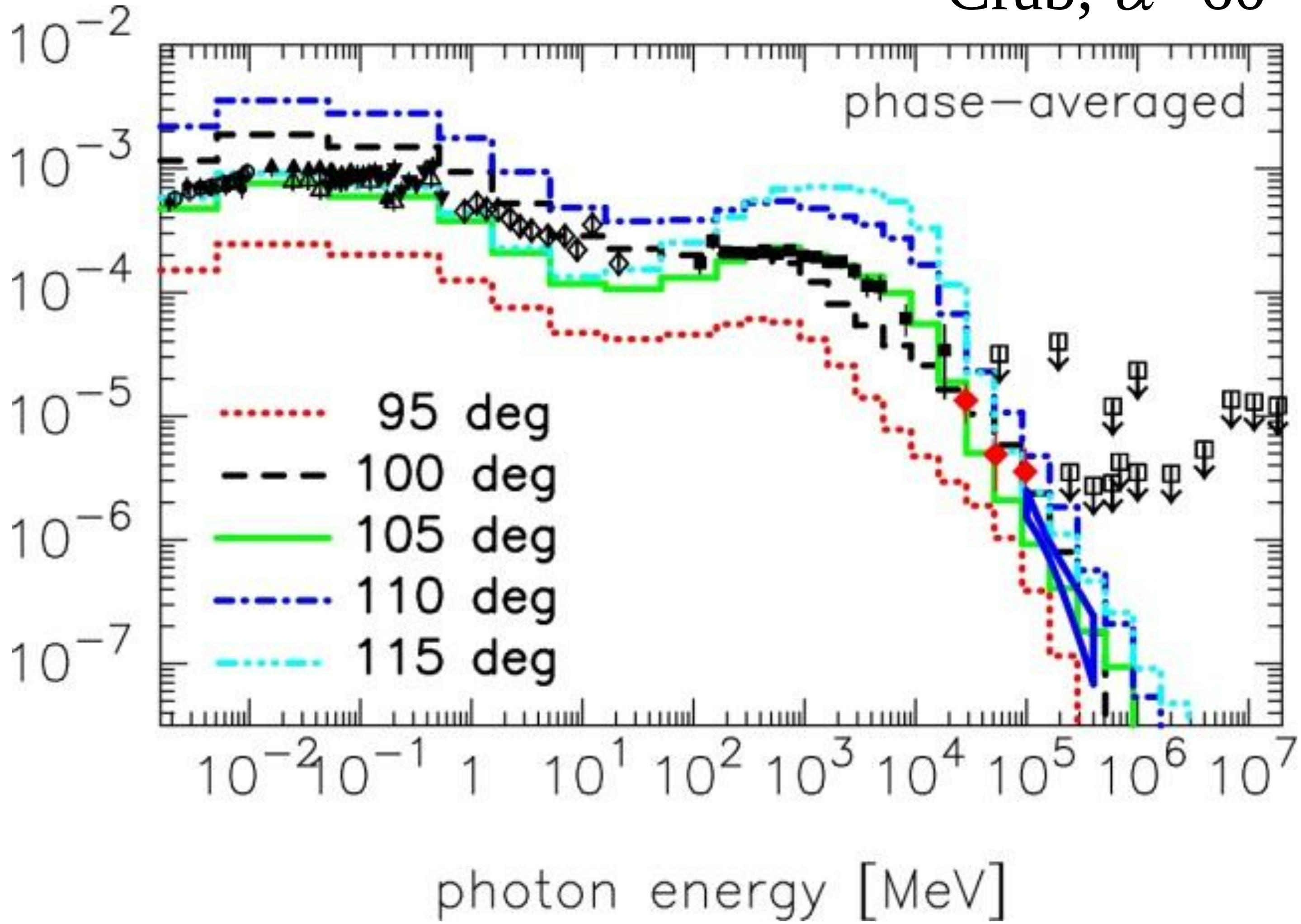

Schematic picture of cascading pairs and their emissions:

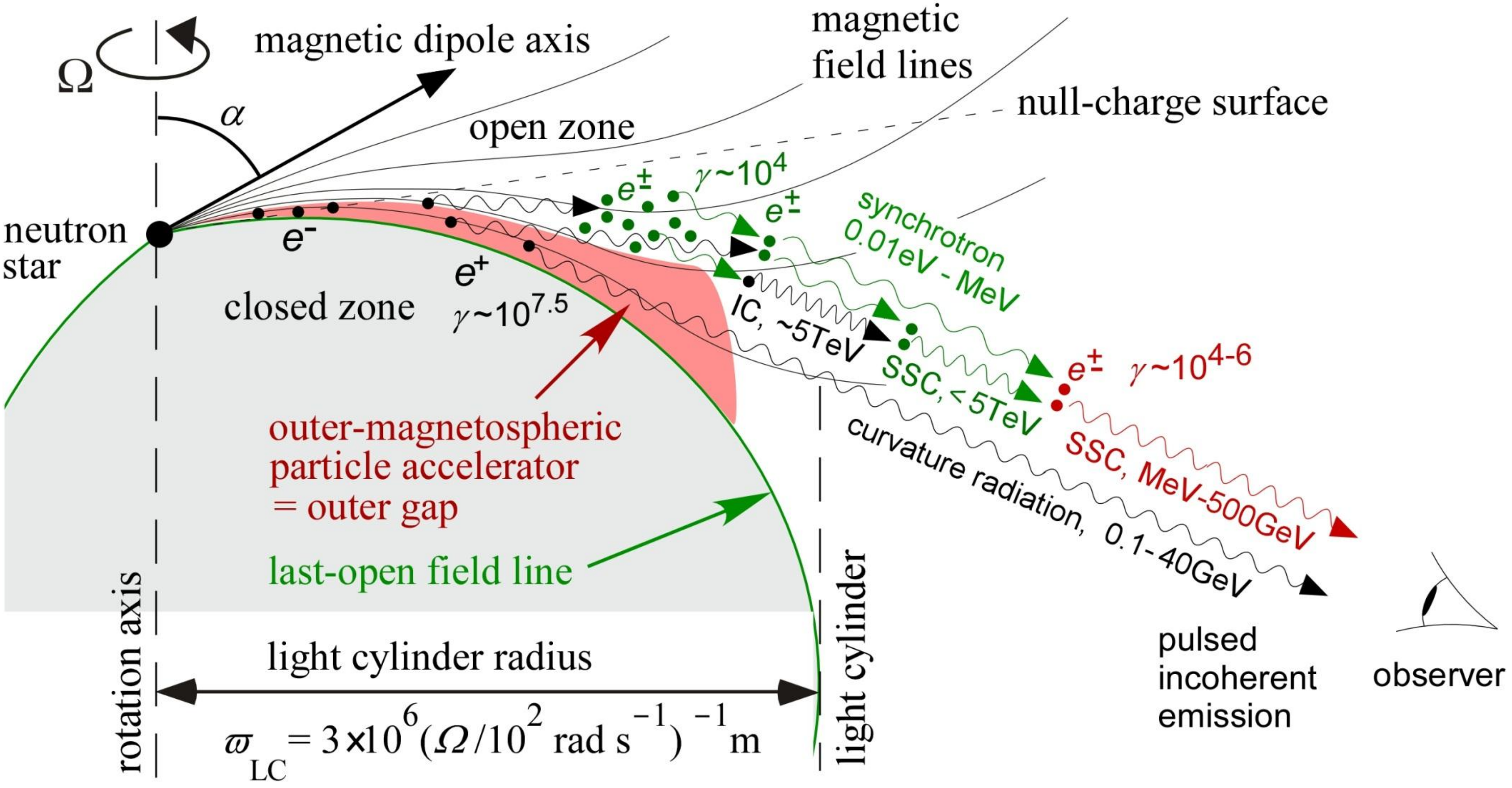

Schematic picture of cascading pairs and their emissions:

Unfortunately, the IC flux is vulnerable to ***B*** geometry near LC.

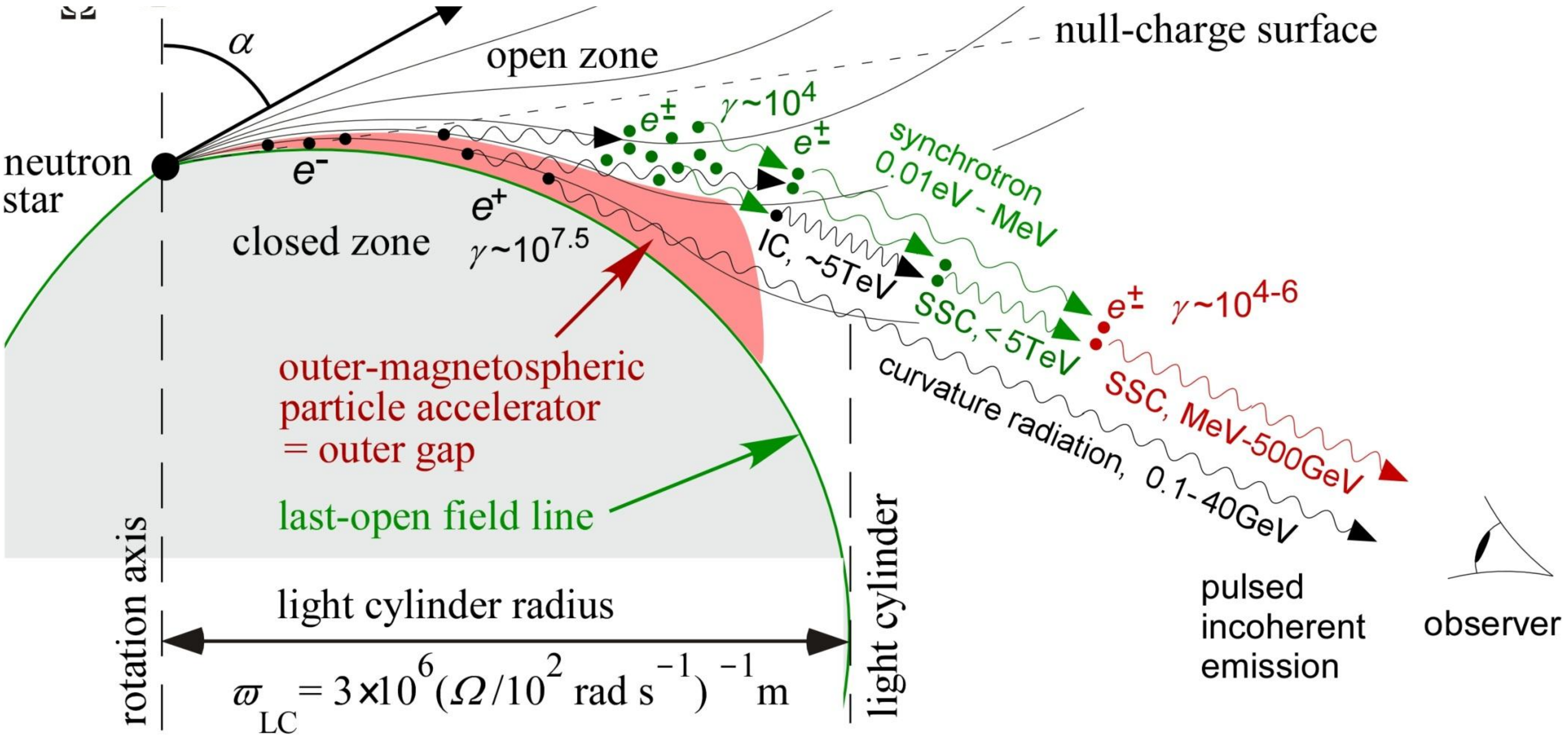

Schematic picture of cascading pairs and their emissions:

Unfortunately, the IC flux is vulnerable to ***B*** geometry near LC.

Incorporation of correct ***B*** geometry near LC is crucial.

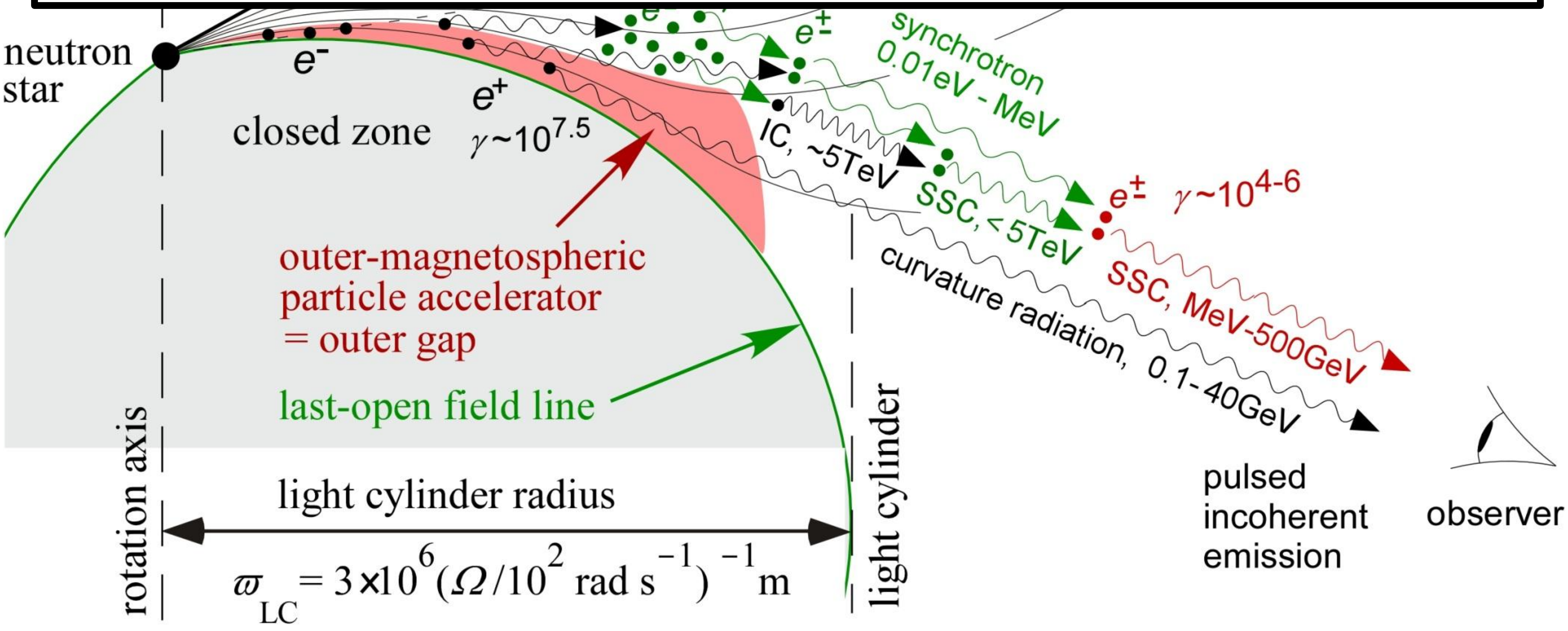

§9 *Theoretical derivation of* $L\gamma \sim L_{spin}^{0.5}$

Let us finally derive the observed relationship, $L_\gamma \propto L_{spin}^{0.5}$, both analytically and numerically.

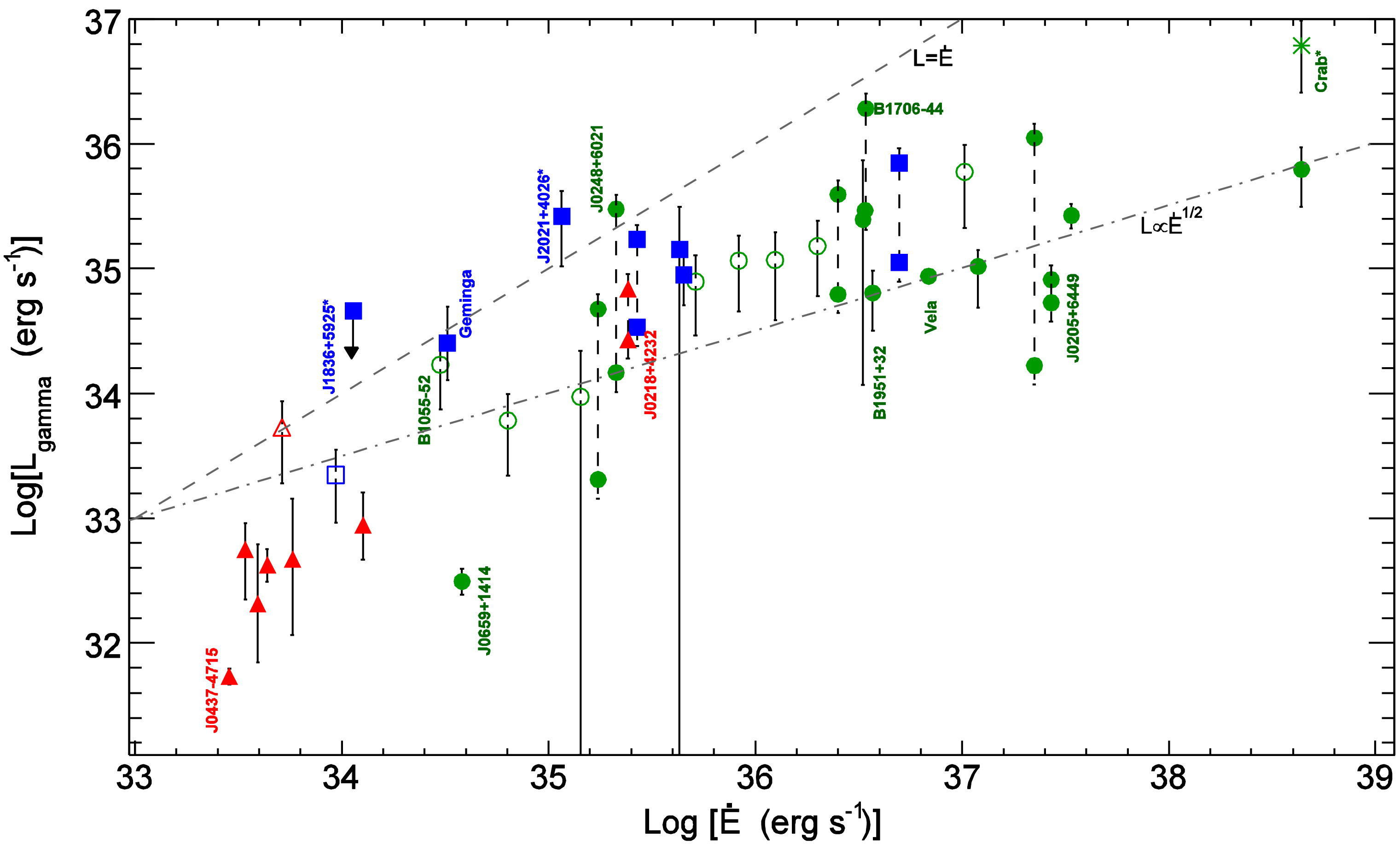

LAT 1st catalog (Abdo+, 2011)

§9 Theoretical derivation of $L\gamma \sim L_{spin}^{0.5}$

To specify the γγ pair production rate, which governs gap evolution, we adopt the minimum cooling scenario.

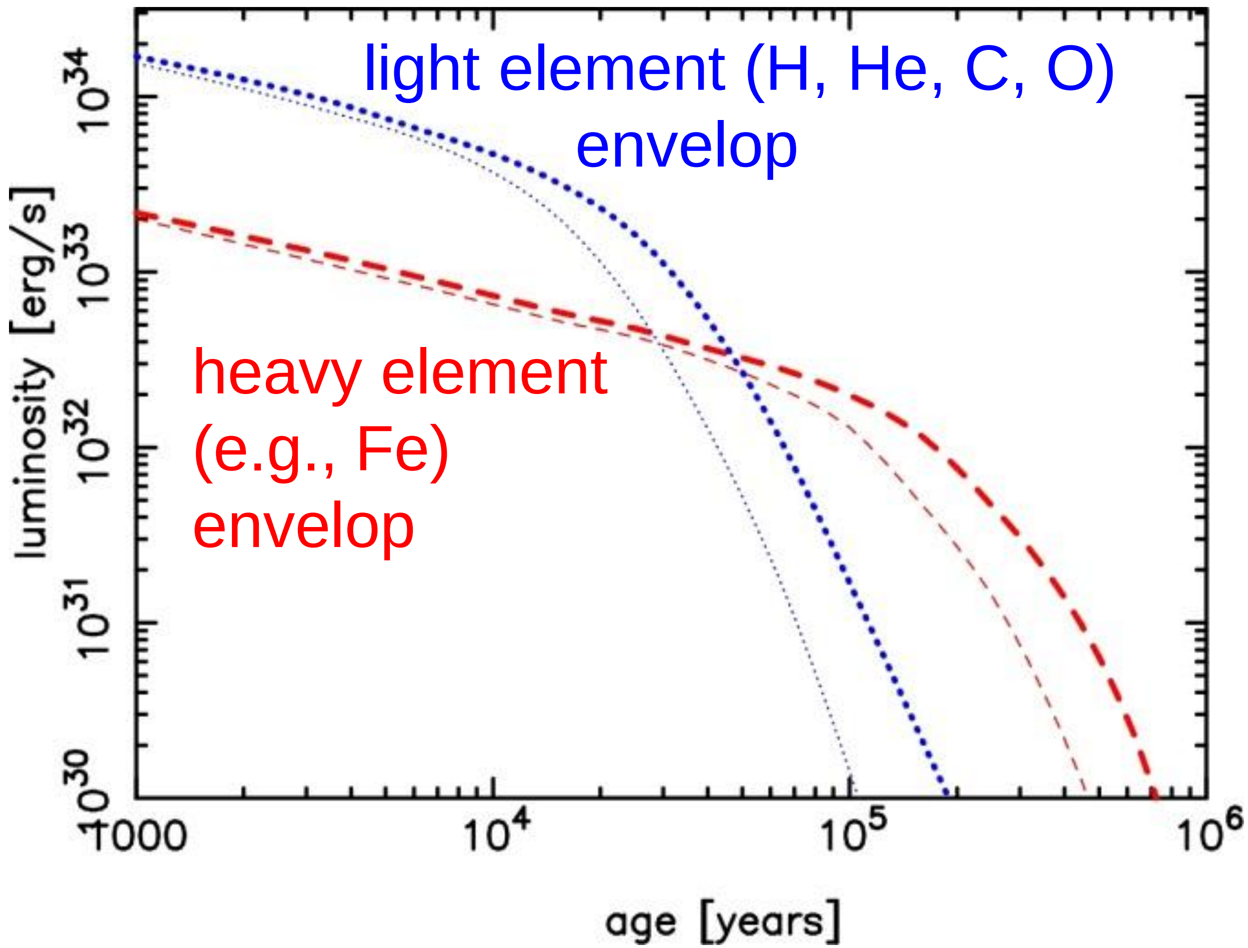

Minimal cooling scenario (Page + 2004)

Gap closure condition, $(N_\gamma \tau)_{in}(N_\gamma \tau)_{out} = 1$, gives analytical predictions of L_γ evolution.

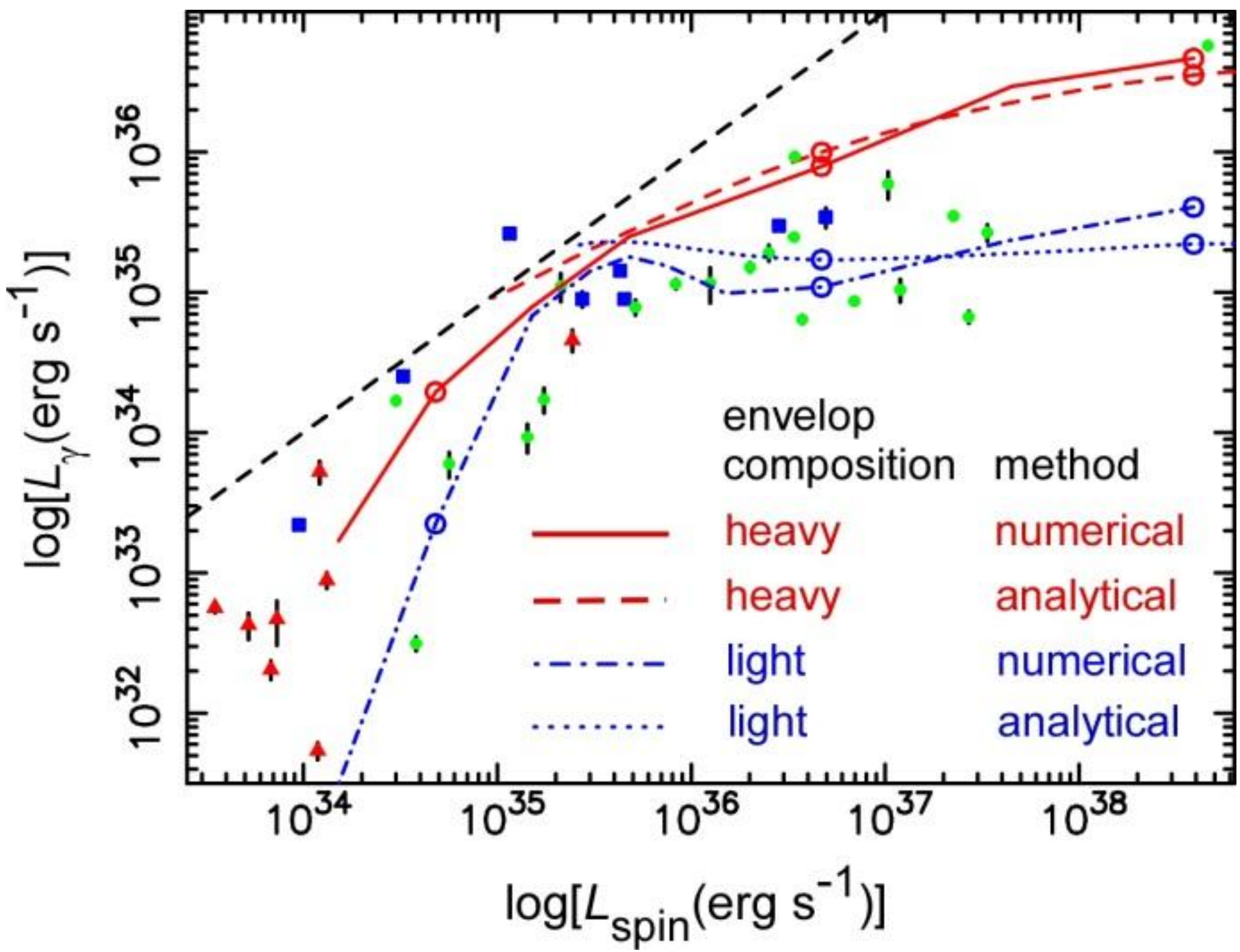

§9 *Theoretical derivation of* $L\gamma \sim L_{spin}^{0.5}$

Also derive L_γ evolution **numerically**, considering both **cooling NS emission** & **heated PC emission**.

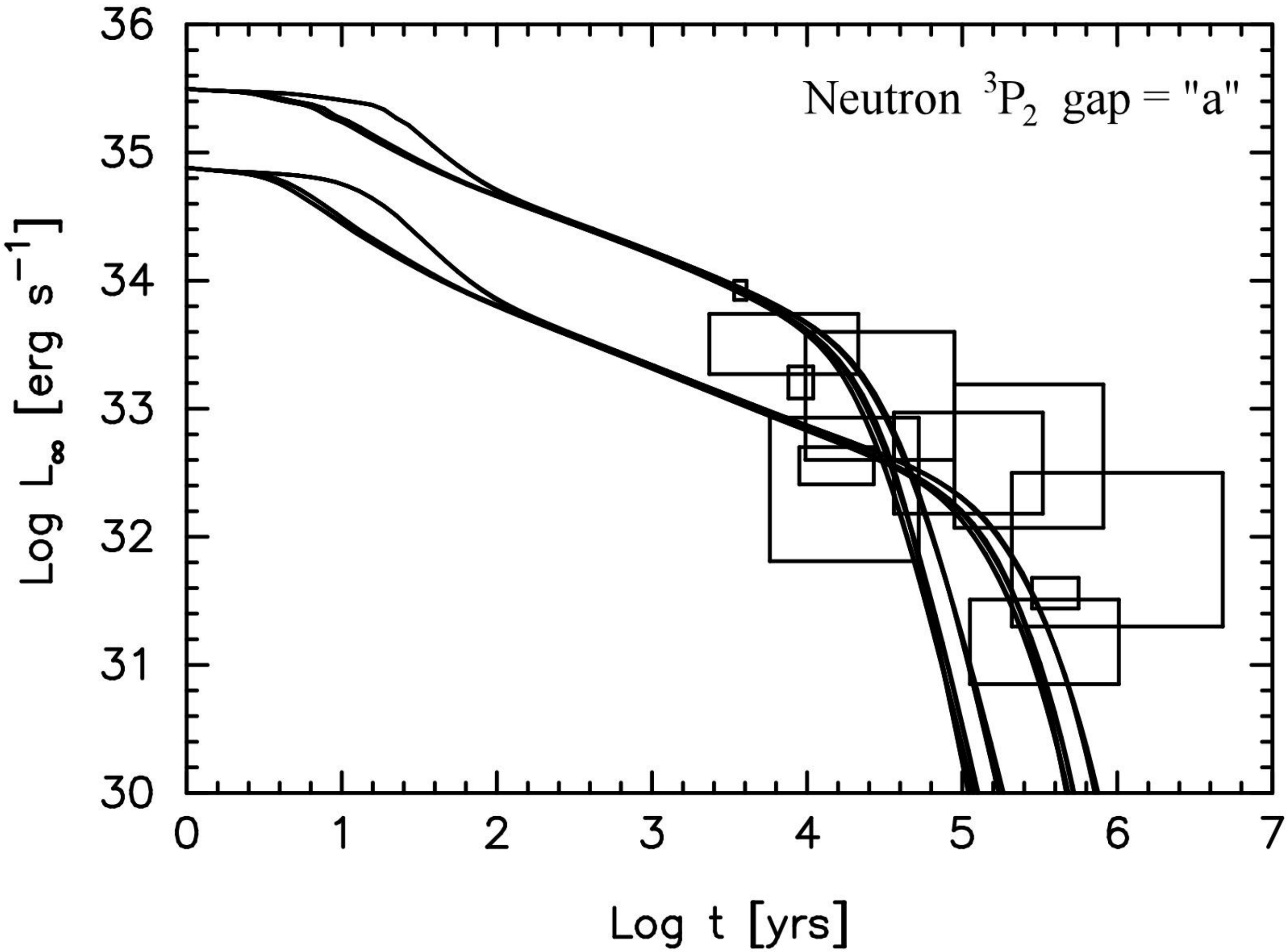

§9 Theoretical derivation of $L\gamma \sim L_{spin}^{0.5}$

Numerical solution is consistent with analytical one.

Greater $L\gamma$ than analytical ones.

Because emission from higher altitudes (LS:P1 & TS:P2) also contribute, in addition to lower altitudes (bridge).

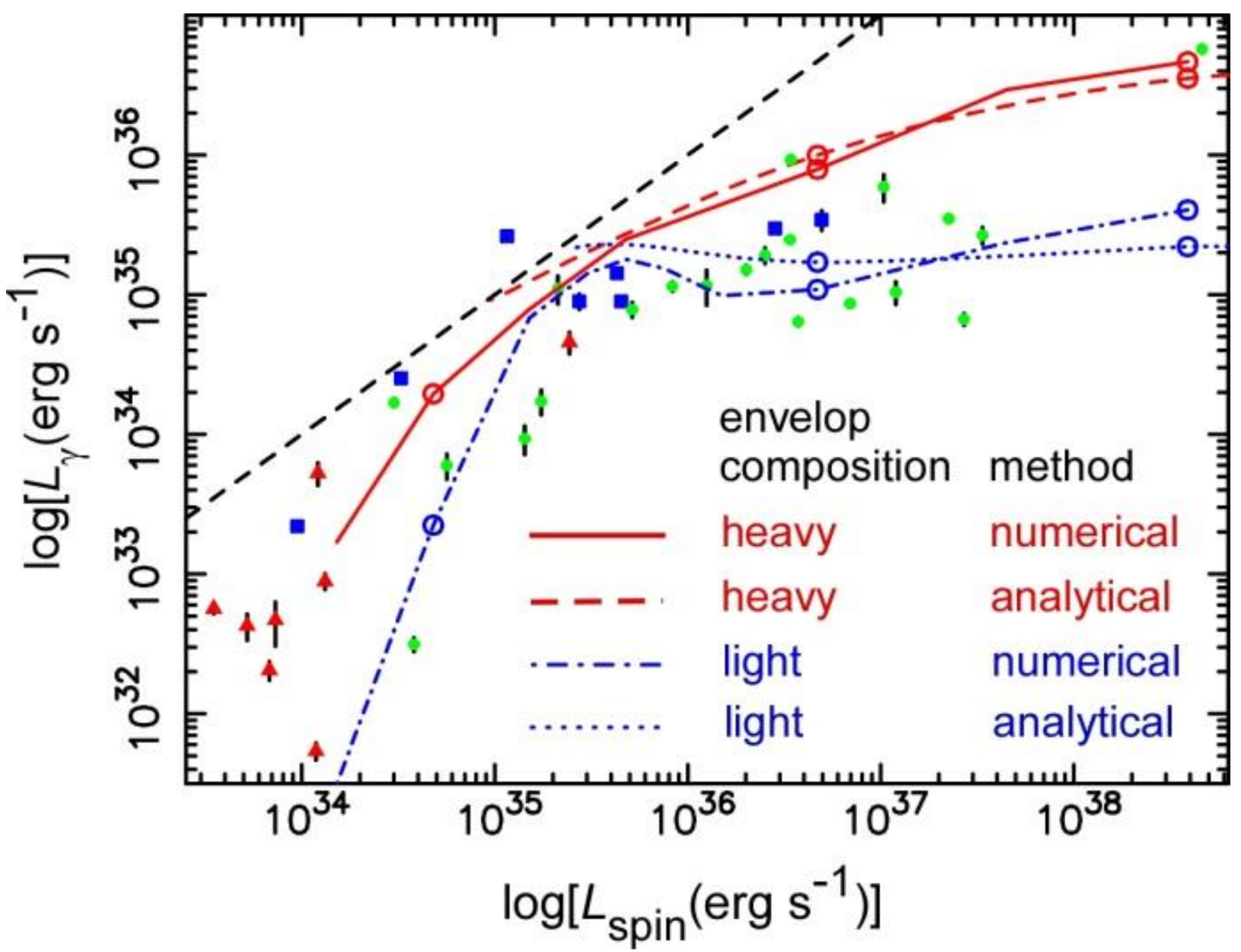

§9 Theoretical derivation of $L\gamma \sim L_{spin}^{0.5}$

Numerical solution is consistent with analytical one.

ρ declines at L_{spin}<10^{35} erg/s

↓

$L\gamma$ declines sharply.

For light element envelop, $L\gamma$ peaks around 30000 yrs, as predicted by analytical calculation.

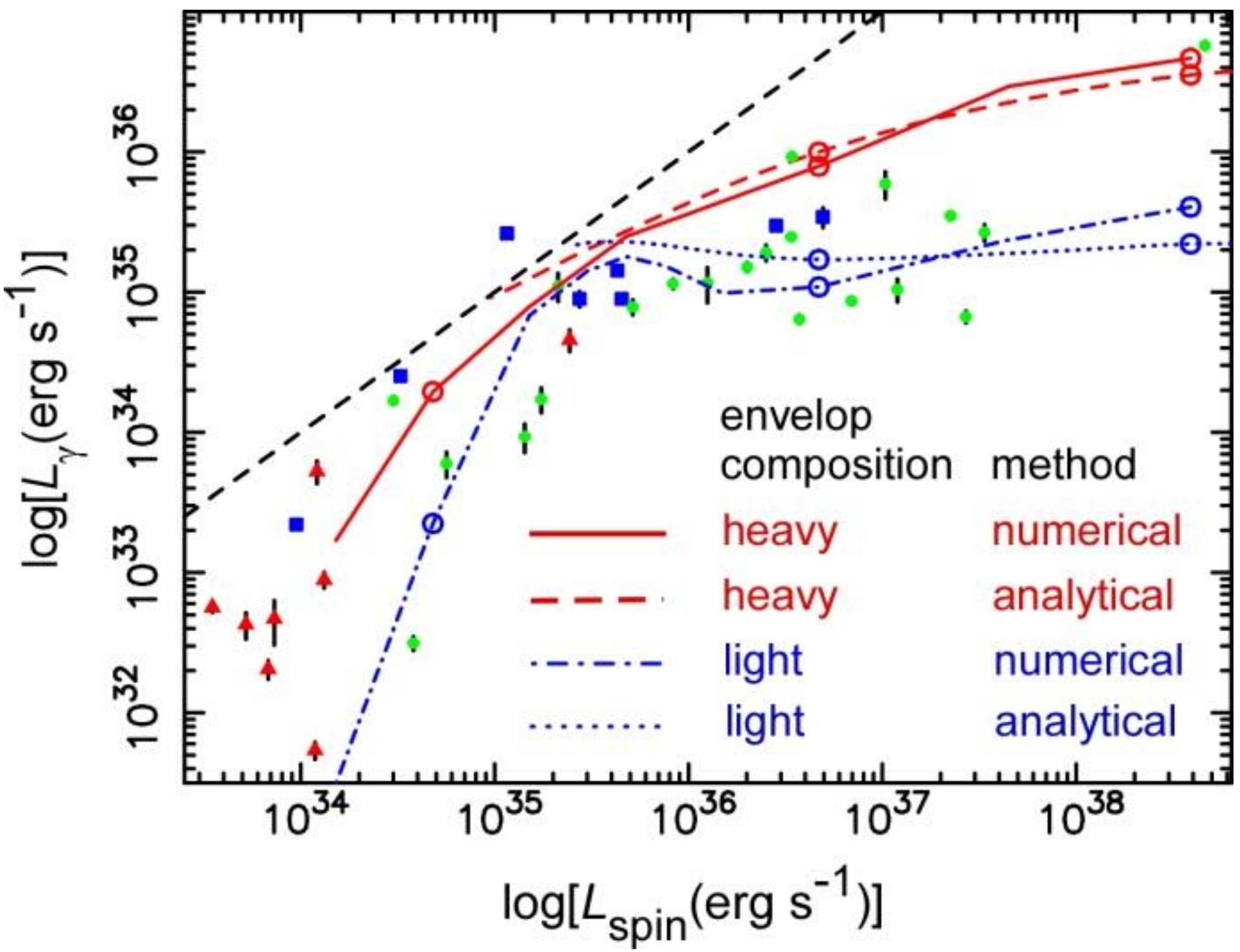

§9 Theoretical derivation of $L\gamma \sim L_{spin}^{0.5}$

Numerical solution is consistent with analytical one.

A realistic NS will have envelop composition between the two extreme cases, light and heavy element envelops.

Thus, the actual L_γ will distribute between the red and blue curves.

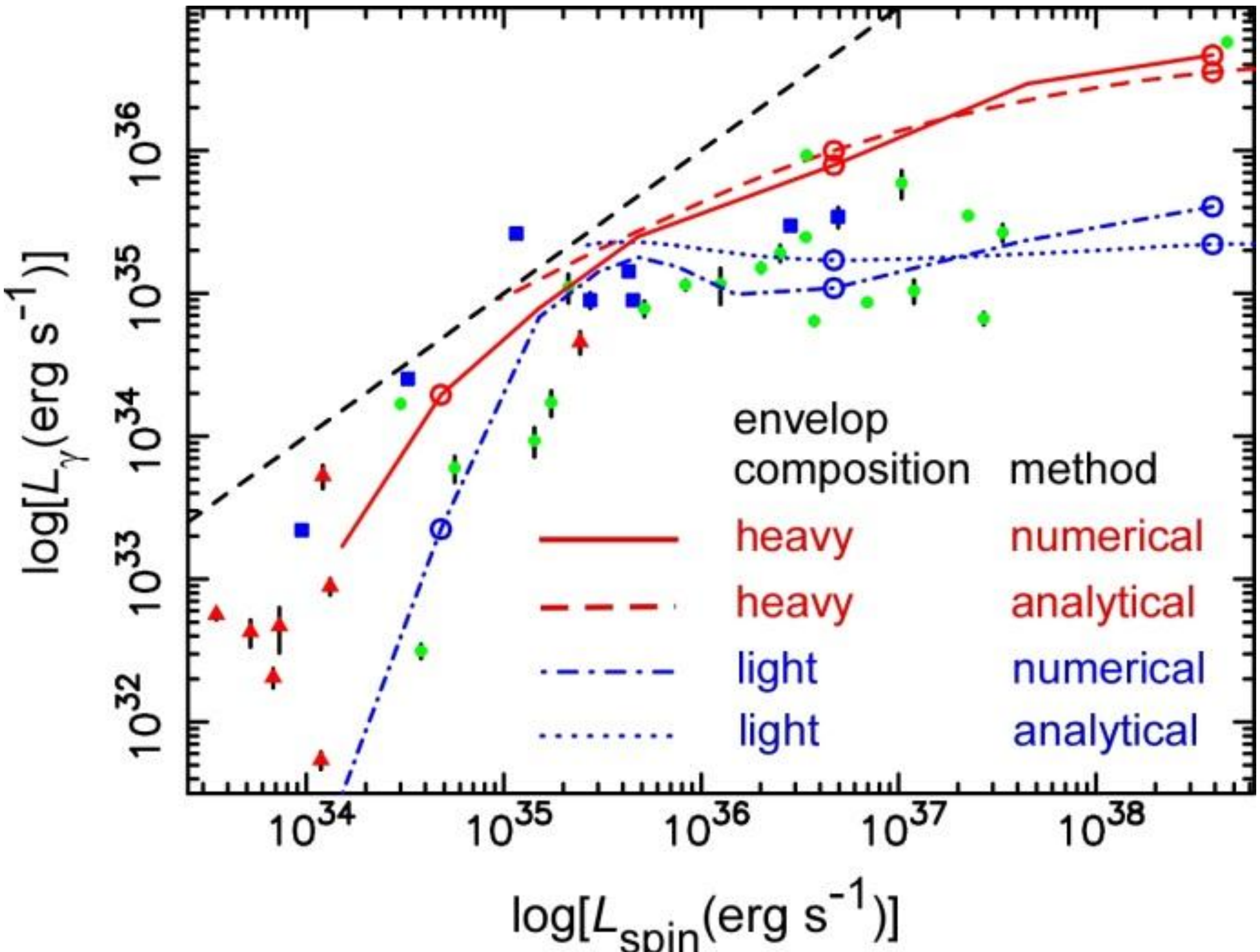

Summary

- We can now solve pulsed high-energy emissions from the set of Maxwell (div$\boldsymbol{E}=4\pi\rho$) and Boltzmann eqs., if we specify P, dP/dt, α_{incl}, kT_{NS}. We no longer have to assume the gap geometry, $E_{\parallel}$, $e^{\pm}$ distribution functions.
- By SSC of secondary/tertiary pairs, Crab pulsar's total and phase-resolved spectrum shows a power-law-like shape.
- Observed relationship, $L_{\gamma} \propto L_{\mathrm{spin}}^{0.5}$, can now be derived both analytically and numerically under the OG model.